BIAXIAL INVESTIGATION OF PERIOSTEAL MECHANICS

by

OLUMIDE O. ARUWAJOYE

Presented to the Faculty of the Graduate School of

The University of Texas at Arlington in Partial Fulfillment

of the Requirements

for the Degree of

MASTER OF SCIENCE IN BIOMEDICAL ENGINEERING

THE UNIVERSITY OF TEXAS AT ARLINGTON

August 2009

ACKNOWLEDGEMENTS

Firstly, I would like to thank my supervising professor, Dr. Paul Wells, for giving me the opportunity to work with him and continue my never-ending quest for acquiring new knowledge and achieving new goals. I would also like to thank my committee member, Dr. Cheng-jen Chuong, for introducing me to the fine work at Texas Scottish Rite Hospital and his continual support and interest throughout my graduate career. Furthermore, I am grateful for Dr. Robert Eberhart for also serving in my committee and expressing interest in the study.

I would like to thank Texas Scottish Rite Hospital for its countless resources and helpful staff. Also, I am very appreciative to Tracy Wassell and Monya Powell in conjunction with the University of Texas Southwestern Medical Center for their assistance in obtaining tissues used for the study.

I am also grateful of the work done by previous students in order to get to this point. I would like to show gratitude to Daniel Warren for the essential framework for this study, to Phillip Ashley for his contribution to motion analysis, and to Thomas John for experimental development. Also, I am very appreciative of general guidance provided by Dr. Jay Humphrey.

I would like to also thank my family and friends that have supported me throughout my academic career. Your support for education has made life all the more intriguing.

July 17, 2009

ABSTRACT

BIAXIAL INVESTIGATION OF PERIOSTEAL MECHANICS

Olumide O. Aruwajoye, M.S.

The University of Texas at Arlington, 2009

Supervising Professor: Paul B. Wells

Limb lengthening procedures are used commonly to correct limb length discrepancies. Current methods in limb lengthening require a distraction of 1 mm per day using an external fixation device. Although the underlying mechanisms of new bone growth have been studied and discussed extensively, they remain not fully understood. It is thought, however, that mechanoreceptor cells of the periosteum play an important role. In an attempt to understand the contribution of periosteum, the biaxial mechanical properties of the periosteum are studied. Freshly excised porcine periosteum was used to investigate the effects of preload on the material symmetry, and the effects of mechanical boundary constraints on the remodeling of the periosteum *in vitro*. The mechanics of porcine periosteum show a greater influence of elastin in its *in vivo* state, and is shown to be highly stressed contrary to other findings. Tissues were cultured in a relaxed configuration, a stretched (*in vivo*) configuration, and a dynamically loaded condition and show trends of increased extensibility over time. A 5-parameter pseudo-strain energy function was employed to characterize the mechanical properties of porcine periosteum. The model was found to fit well for periosteum tested from a relaxed preconditioned state, but was unable to predict corresponding *in vivo* and proportional responses.

TABLE OF CONTENTS

LIST OF ILLUSTRATIONS

LIST OF TABLES

CHAPTER 1

INTRODUCTION

1.1. Growth and Development of Bone

Growth and development of normal bone has been studied and discussed widely [Klein-Nulend et al., 2005; Robling et al., 2006; Carter and Beaupré, 2001]. Bone growth in long bone (Figure 1.1) occurs in two directions, longitudinally and circumferentially. Longitudinal bone growth takes place through chondrocyte division and hypertrophy at the growth plates [Hunziker et al., 1987; Hunziker and Schenk, 1989; van der Meulen and Huiskes, 2002] and circumferential bone growth develops between the periosteum and cortical surface [van der Meulen and Huiskes, 2002], thereby increasing bone strength during male adolescence [Schoenau et al., 2001]. Mechanobiology, in the context of orthopedics, is the study of how bone grows and develops in response to different types of mechanical stimuli, and conversely, how growth and development affects the mechanical state of bone. For example, during embryonic development, morphology of the skeleton is affected by the directionality and magnitudes of mechanical loading [Carter and Beaupré, 2001]. Thus, the physiologic mechanical environment (dictated largely by the bone's function) affects directly the development (i.e. the form) of bone. This mechanobiological principle can also be exploited clinically.

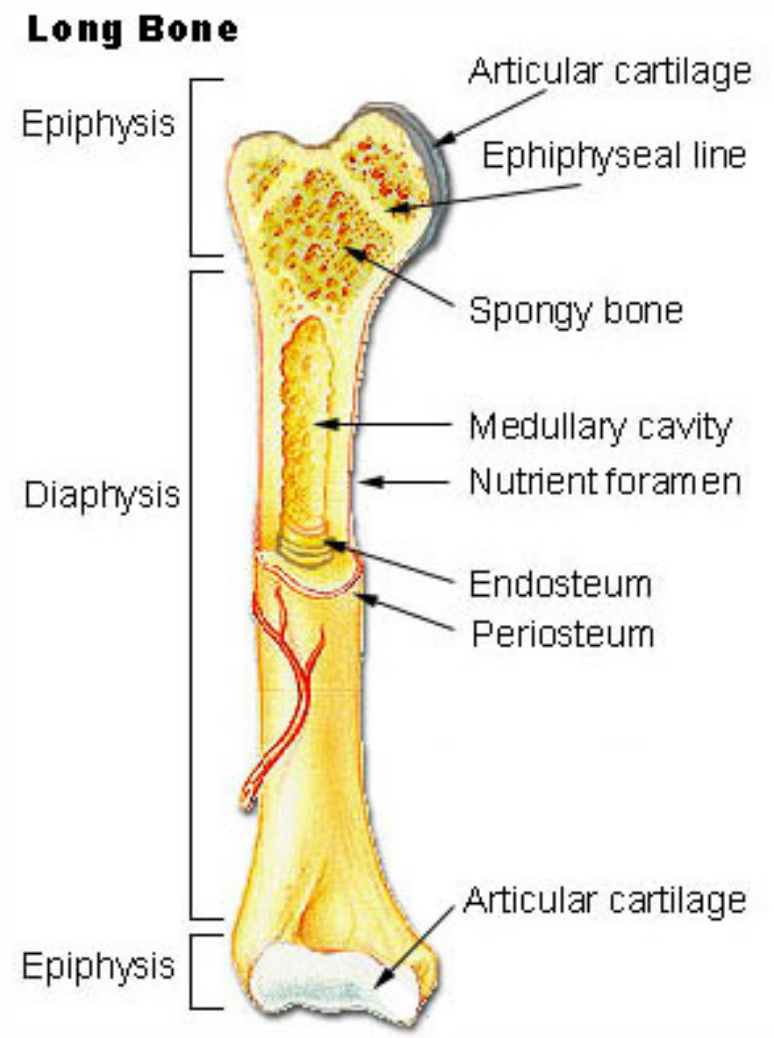

Figure 1.1 Anatomy of a typical long bone
[<http://training.seer.cancer.gov/anatomy/skeletal/classification.html>]

1.1.1 Clinical Procedures

For clinical procedures, understanding and manipulating the mechanobiology of bone is important perhaps most notably during distraction osteogenesis and other forms of fracture fixation. Limb lengthening, a form of distraction osteogenesis, was made popular by the Russian doctor, Gavril Ilizarov, because of his relatively successful technique and system. The Ilizarov technique and system has been studied widely [Paley et al., 1989; Cattaneo et al., 1990;

Ilizarov, 1990; Grant et al., 1992; Birch and Samchukov, 2004] and so, too, have the complications [Paley 1990; Velazquez et al, 1993]. Briefly, the method involves an osteotomy (cut), to create two separate bone segments. The two bone segments are then fixated externally (Figure 1.2), allowed to initiate the healing process for approximately seven days, and then separated at a prescribed rate until the desired length is obtained or physical limitations are reached.

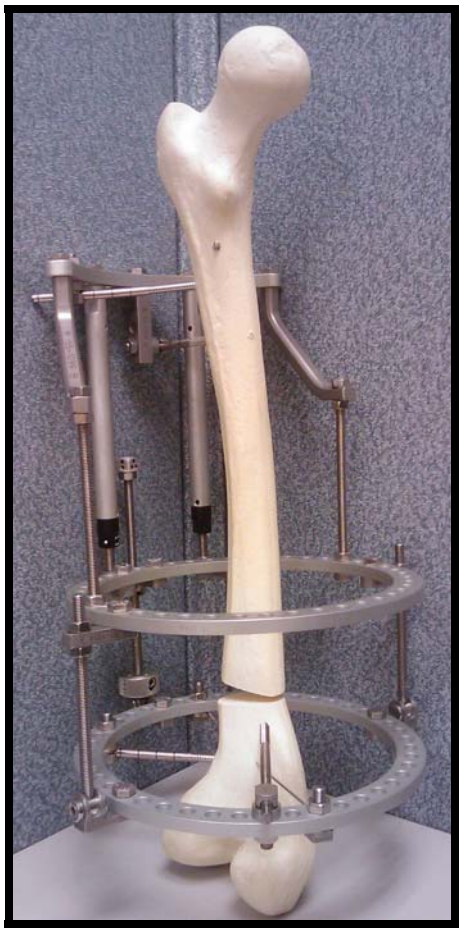

Figure 1.2 Model of a femur with an external fixation system

Experimental data and anecdotal evidence suggest that 1 mm of distraction per day achieves optimal new bone growth for the majority of patients [Birch and Samchukov, 2004]. For some patients, however, distraction should be faster or slower to avoid common

complications associated with lengthening, such as premature consolidation or poor regenerate [Ilizarov, 1990]. Clearly, then, one burden of future research is to determine what factors dictate the optimal distraction rate and/or healing. For example, we know that optimal new bone growth will more likely occur when surrounding soft tissues are well preserved throughout surgery and distraction, as they promote good bone healing [Yasui et al, 1993], yet little is understood regarding the mechanisms of soft-tissue involvement. Specifically, we would like to know if the mechanics of the soft tissues affect bone growth [Markel et al., 1990], and if those mechanics shed light on why the method is more effective on some and not others. Understanding the mechanics of soft tissue on a patient specific basis, then, could yield a more optimal treatment for all patients. This begs the question of which soft tissue is most important during limb lengthening.

1.1.2 Key tissues

Structurally, from the outer surface to the center, long bone is typically composed of periosteal, cortical, endosteal, and cancellous layers. The key soft tissues involved are the periosteum and endosteum, both of which have documented roles in bone healing and skeletal regeneration [Carter et al., 1998; Pacicca et al., 2003; Görtz et al., 2004] Compared to the endosteum, the periosteum has garnered much more attention because of its relatively larger quantity of osteogenic cells [Takushima et al., 1998; Redlich et al., 1999; Allen et al., 2004], its importance for cortical blood supply [Decker et al., 1996], and the fact that most new bone originates at the periosteal surface [Kojimoto et al., 1988; Carter et al., 1998]. Some focus on the periosteum has been on a cellular level [Tenenbaum et al., 1986; Redlich et al., 1999; Takushima et al., 1998], where cells were cultured *in vitro* and seeded to induce bone growth. Cells were noted not to obtain a callus formation without mechanical stimuli of the environment [Takushima et al., 1998]. Of course, several other tissues that surround the bone (e.g. muscle, nerves, skin) may also play an integral role in distraction osteogenesis, but they are beyond the scope of this study. For this reason, our focus herein is the periostuem.

1.2 Periosteum

1.2.1 Role in Mechanobiology of Bone

Because of an established role in healing and development of bone [Grundnes and Reikerås, 1993; Carter et al., 1998; Utvåg et al., 1998], and modulation of longitudinal bone growth via a mechanical tethering effect over growth plates [Warrell and Taylor, 1979; Houghton and Dekel, 1979; Houghton and Rooker, 1979; Lynch and Taylor, 1987], incision of the periosteum has been evaluated for surgical procedures. Specifically, the circumferential release of the periosteum has been described well for correction of leg length inequalities, with noted complications [Wilde and Baker, 1987; Al Hussainy et al., 2004]. Generally, circumferential strips of periosteum overlying the growth plates were excised. This periosteal "release" is thought to accelerate bone formation because of the reduced preload on the growth plates [Warrell and Taylor, 1979]. This, of course, has led to questions of what loads are experienced by the periosteum while *in vivo.*

1.2.2 Mechanics of Periosteum

No study has fully characterized the mechanical properties of periosteum. Tensile properties were measured for the longitudinal axis of avian bone [Bertram et al., 1998], tensile failure was evaluated for multiple locations of periosteum from long bone [Uchiyama et al., 1998], and craniofacial regions [Popowics et al., 2002] of porcine periosteum, and three-point bending of long bone was performed to measure the contribution of periosteum to the mechanical properties of whole long bone [Yiannakopoulos et al., 2008]. None of the aforementioned studies, however, evaluate typical *in vivo* conditions experienced by the periosteum. Indeed, they all use extraphysiologic and uniaxial loads.

Because long bone grows both longitudinally and circumferentially, periosteum naturally experiences loads in two primary directions. Furthermore, residual biaxial strains in the periosteum correlate with local growth rate [Chen et al., 2008]. Thus, periosteum should be tested multiaxially to simulate more closely the true *in vivo* loading. Biaxial testing is of particular

interest herein because of prior experience in our lab, and because the mathematical and experimental complexities can be reduced to 2D by way of the membrane theory of continuum mechanics. Hence, biaxial testing simplifies constitutive relations and allows better estimation of material parameters [Lanir et al., 1996] using phenomenological and/or microstructural approaches to modeling.

Indeed, mechanics of collagenous tissues have been described by the microstructural approach [Lanir, 1979, 1983; Billiar and Sacks, 2000], which seeks to describe material parameters from the physical nature [Lanir, 1983; Humphrey and Yin, 1987], and phenomenological models [Tong and Fung, 1976; Chew et al., 1986], which rely on data from gross mechanical experiments to develop a constitutive equation [Humphrey and Yin, 1987]. While the microstructural approach seems to be the more appropriate descriptor in principle, the models can become quite complex. Meanwhile, the phenomenological approach may result in physically meaningless parameters, non-uniqueness or other mathematical inconsistencies [Humphrey and Yin, 1987]. This, logically, has led to hybrids of the two approaches in modeling [Humphrey and Yin, 1987; Kuhl and Holzapfel, 2007]. Regardless of the approach, accurate material parameters for soft tissues can only be garnered with the continued pursuit of better constitutive equations, along with appropriate experimentation.

1.3 Specific Aims

This study aims to determine the effects of preload on the material symmetry, identify a constitutive model that represents that data well, and study the effects of mechanical boundary constraints on the remodeling of porcine periosteum *in vitro*.

CHAPTER 2

METHODS

2.1 Specimen Preparation

2.1.1 Dissection and Mounting

Our specimen preparation is similar to that described by Warren (2008). Briefly, tissues were obtained from farm pigs within approximately one hour of euthanasia, using aseptic techniques and sterile tools. Age, weight, and sex of the pigs were unavailable. First, the anteromedial portion of the pig ulna was identified for incision. After removal of skin, tissue and fascia to expose the periosteum, great care was taken to note the longitudinal and circumferential axes of the tissues. Each sample was cut approximately 15 X 15 mm and measured accordingly with a measuring tape (before removal). Finally, the periosteum was gently removed from the bone with a periosteal elevator, placed in a media-filled conical, and prepared for mounting as described below.

The samples were removed from the conicals and floated in a shallow Petri dish so that their traction-free dimensions could be measured via digital imaging. Then, they were placed on an EPDM (ethylene propylene diene M-class rubber) foam frame with the cambium layer facing up. Custom-formed stainless steel hooks were attached through the tissues into the EPDM foam frame. With three evenly-spaced hooks per side, the tissue-foam-hook construct was transferred to the biaxial chamber (described in 2.2.1) and aligned according to the appropriate axis. Sutures within the biaxial chamber were placed carefully on each hook and tensioned for engagement to the tissue-foam-hook construct so that the foam could be removed gently from the hooks, leaving the tissue suspended like a trampoline. Next, the chamber was placed under a stereo microscope to visualize the placement and gluing [Vetbond 3M St. Paul, MN] of four

crushed particles of black rock [Hobby Lobby Oklahoma City, OK] (~200 μm each) to the surface of the tissue, forming an approximate 1 X 1 mm square in the central region. The glue was allowed to cure for a couple of minutes prior to addition of media [DMEM, High Glucose 1X Sigma-Aldrich St. Louis, MO], which completely submerged the tissue.

2.2 Experiments

2.2.1 Mechanical Testing Device

We used the same devices described well by Warren (2008). Briefly, the device consists of a cruciform shaped chamber that is filtered, oxygen perfusable and fully autoclavable. Within the chamber, there are two orthogonally positioned beam-type load cells: one for each axis. Each load cell is attached inferiorly to a suture bracket used to engage the tissue hook construct. Superiorly, each load cell is attached to another bracket that engages 2 rods that penetrate the chamber to be engaged by a push plate. On the opposing side of each axis are “dummy” brackets, which are brackets without load cells. The “dummy” brackets are engaged in a similar fashion.

The chamber sits on an aluminum plate that is engaged by four orthogonally placed stepper motors, and the plate sits atop a Kaiser platform [Kaiser Fototechnik Buchen, Germany]. The Kaiser platform supports an overhead camera used to view the markers glued to the tissues. Figure 2.1 shows the biaxial mechanical testing system.

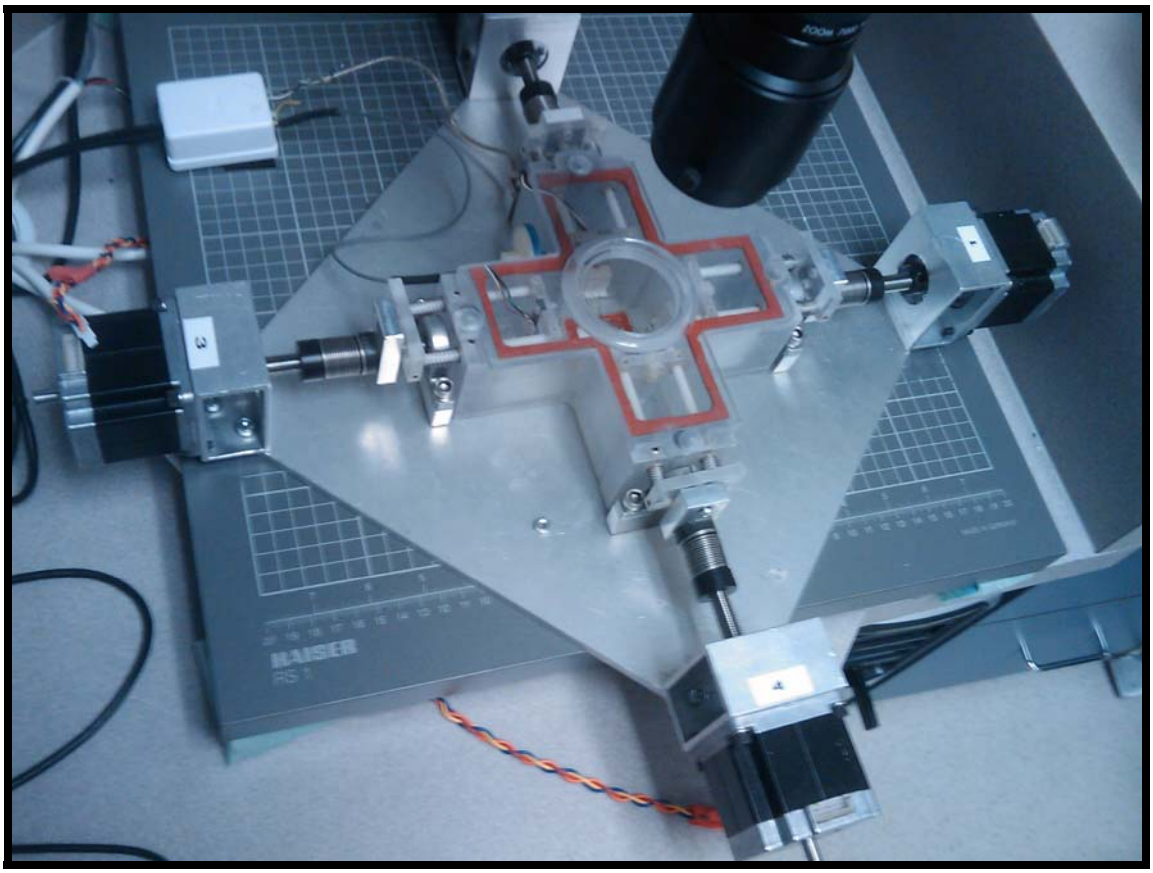

Figure 2.1 Biaxial Mechanical Testing System. Deformation is applied by four opposing stepper motors, forces are monitored through two beam-type load cells (one per axis) and displacements are measured using non-contact overhead visualization of tracking particles.

2.2.2 Computer Controlled Tests

Each stepper motor was controlled independently by a custom code developed in LabVIEW ®. Within the program, four particles were selected and their centroids tracked in view of the camera for a non-contact monitoring of the displacement. The algorithm, within the code, enabled calculation of strain, based on the movement of the four particles. The loads were monitored from the two aforementioned load cells. Limits of stretch (calculated from displacement) and loads were set prior to testing for feedback control of the device.

The updated positions of the particles were calculated from position vectors x and X which are defined in Equation 1,

$$x_1 = \lambda_1 X_1 + \kappa_1 X_2, \qquad x_2 = \lambda_2 X_2 + \kappa_2 X_1 \tag{1}$$

where λ_i is an estimation for the axial stretch ratio and κ_i is a measurement of shear and other changes with rigid body motions (e.g. rotations) . These position vectors were used for calculating deformation, which is defined in Equation 2,

$$\mathbf{F} = \begin{bmatrix} \frac{\partial x_1}{\partial X_1} & \frac{\partial x_1}{\partial X_2} \\ \frac{\partial x_2}{\partial X_1} & \frac{\partial x_2}{\partial X_2} \end{bmatrix} \tag{2}$$

where the components of $\mathbf{F}$ are

$$F_{11} = \lambda_1 \qquad F_{12} = \kappa_1 \qquad F_{21} = \kappa_2 \qquad F_{22} = \lambda_2 . \tag{3}$$

All of the components of $\mathbf{F}$ were used in calculations of the principal stretch for data collection, where $\Lambda_1 = \sqrt{F_{11}^{\ 2} + F_{21}^{\ 2}}$ and $\Lambda_2 = \sqrt{F_{22}^{\ 2} + F_{12}^{\ 2}}$. However, for feedback control the λ_1 and λ_2 were used because of the device's inability to control the values of κ_1 and κ_2. It should be noted that the values of κ_1 and κ_2 were negligible during testing (see Table 2.1), as care was taken to stretch tissues along the corresponding longitudinal and circumferential axis, and to minimize rigid body motions. Table 2.1 shows values for κ_1 and κ_2 close to zero.

Table 2.1 Averaged κ_1 and κ_2 values for each tissue.

Tissue Number	κ_1	κ_2
1	0.03970913	0.053948773
2	0.032792914	0.033774617
3	0.014601648	0.017664914
4	0.032377117	-0.020008313
5	0.002983164	0.030318994
6	0.054614135	0.060212567
7	0.021418236	0.035908177
8	0.039786655	0.011541479
9	0.007686957	0.088307561
10	0.011634952	0.050145353
11	-0.010894417	-0.00151189
12	0.013998312	0.029593154
13	0.00205294	0.020120827
14	0.040556156	0.075035999
15	-0.001930967	0.029002019
16	-0.008501177	0.002618624
17	-0.001541837	0.029621683
18	0.063378207	0.062300236
19	-0.030597772	-0.018010348
20	-0.005858576	0.027847649
21	-0.006519164	-0.024394824
22	0.030971758	0.042476755
23	-0.002690904	0.026085818
24	-0.00202286	0.053729677
25	0.03970913	0.053948773
26	-0.014370598	0.010939758
27	0.005323185	0.00466396
28	-0.00057344	0.030926076

Within 24 hours of excision, each tissue underwent specific test protocols for characterization and modeling. Initially, the tissue was relaxed fully (no tension in the sutures) and the relaxed reference configuration was recorded; the tissue was preconditioned for 5 cycles between 5g and 80g of load equibiaxially. Next, a relaxed preconditioned configuration was recorded (β_P), and an equibiaxial-stretching test was performed, wherein the stretch ratios for both axes were kept equal for 3 cycles of testing with an upper load limit of 80g and a lower limit of λ_{min}=1.05. Next, the tissue was displaced to its maximum stretch along the longitudinal

axis (Constant-Y protocol) and cycled along the circumferential axis between a lower stretch ratio of λ_{min}=1.07 to an upper limit equaling the max stretch achieved during the equibiaxial protocol. The test was completed again with axes reversed (Constant-X). Then, a proportional test was performed wherein the longitudinal axis was strained twice that of the circumferential axis for a lower limit of $\lambda_{min\text{-}x}$=1.05 for the circumferential axis and $\lambda_{min\text{-}y}$=1.1 for the longitudinal axis with an upper limit of 80g.

Finally, the tissue was tested equibiaxially in reference to its *in vivo* dimensions. Because previous data shows differential shrinkage of the periosteum in the circumferential and longitudinal direction [Warren, 2008], we surmised that the material symmetry would appear quite different with respect to the *in vivo* dimensions (configuration). The necessary stretch ratios for determining *in vivo* configurations relative to traction-free configurations were determined from the change in dimensions of the tissue from its measured *in vivo* dimensions to its measured relaxed dimensions. Once stretched to its approximate *in vivo* dimensions, the configuration (β_{IV}) was recorded and the tissue was relaxed and stretched equibiaxially for 3 cycles with an upper load limit between 80g and 150g and a lower stretch ratio limit of typically λ_{min}=0.80.

2.2.3 Experimental Groups

Four to six tissues were obtained from each pig (two or three samples per limb), each identified based on location: the proximal, medial, and distal (Figure 2.2). Twenty-eight tissues were tested from 6 pigs, according to the aforementioned procedures, and of those, 12 were cultured and tested at two additional time points (Day 2 and Day 7) for our in vitro remodeling study, described below.

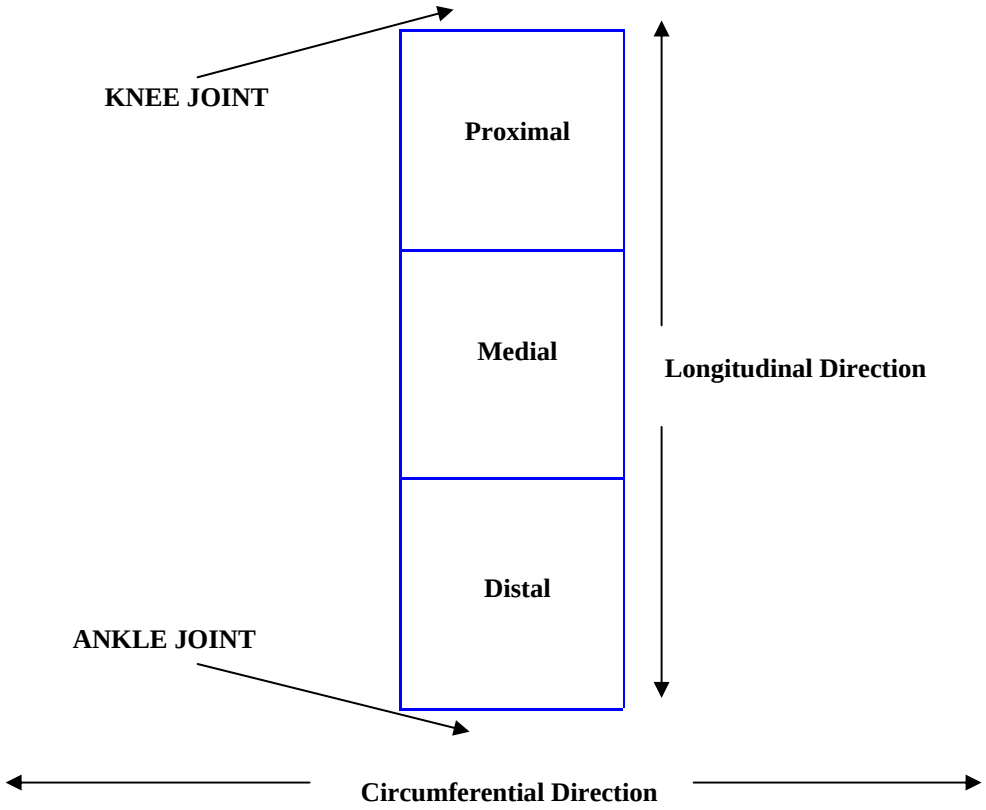

Figure 2.2 Dissection locations of excised periosteum.

2.2.4 In Vitro Remodeling

The remodeling portion of the study dealt with different incubated constraints. After mounting the tissue and immersing it in media, the initial mechanical test occurred within 6 hours (Day 0). Then, the chambers were incubated, and retested approximately 48 hours (Day 2) and 168 hours later (Day 7). Care was taken to keep the tissue in sterile conditions during testing; however, there was some occasional exposure to unfiltered air when the Petri lid was removed due to condensation on the lid post-removal from the incubator. The removal of the lid allowed for more feasible tracking of the particles. While in incubation, each tissue was held under a prescribed mechanical constraint. The *in vivo* constraint maintained the tissue in a stretched state similar to its *in vivo* dimensions. The relaxed constraint maintained the tissue in a completely relaxed state (no tension on the sutures). The final constraint was dynamic, and

was made to cyclically relax and stretch between stretch ratios of approximately 0.8 and 1.0 relative to β_{IV}, at an approximate frequency of 0.2 Hz during incubated periods, using a dynamic biaxial loading platform similar to what is presented in Humphrey et al. (2008). The platform (Figure 2.3) was designed to fit inside the incubator. Atop a polycarbonate base is a DC motor [Model GM9413-3 Pittman Harleysville, PA] that controls 4 orthogonally positioned cams that engage the loading arms of the chamber, placed in the center of the platform for synchronized biaxial loading and unloading of the tissue. The DC motor was powered externally by a regulated power supply [Heathkit Model IP-2728] placed externally to the incubator. Upon removal, at the mechanical testing intervals, the dynamic loads were monitored briefly, the chamber was transferred to a computer-controlled platform, and the protocols repeated.

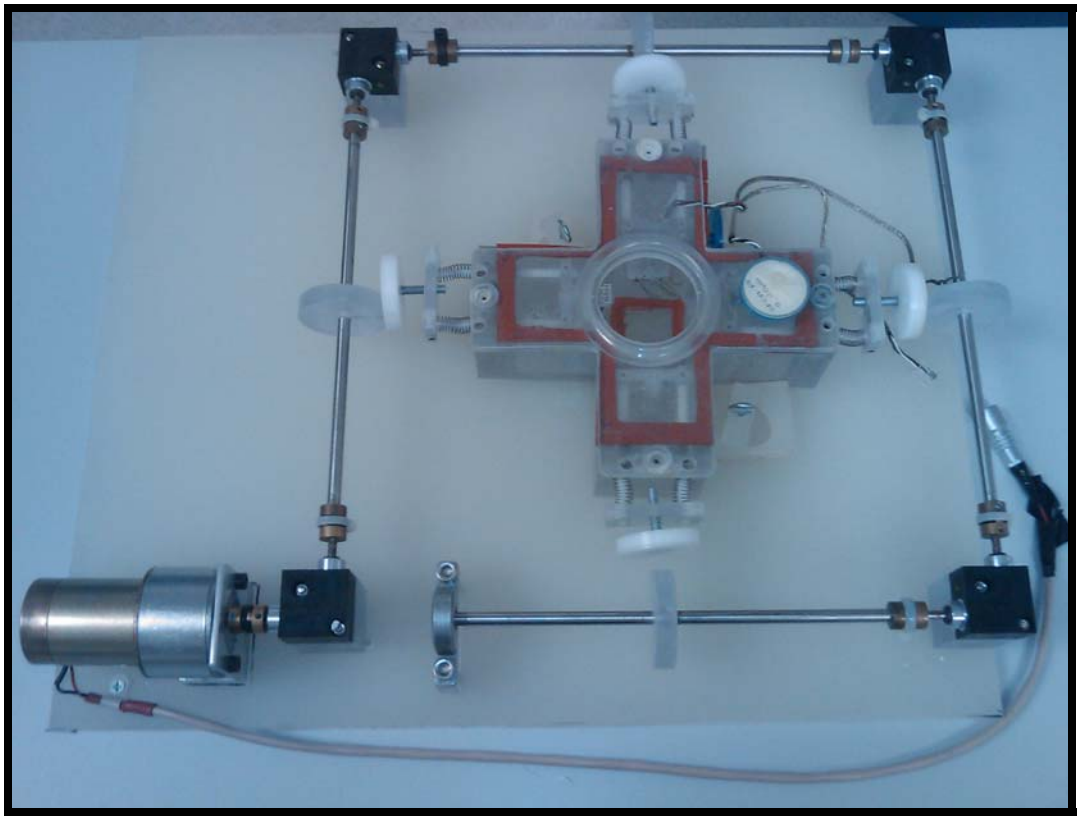

Figure 2.3 A tissue chamber atop the dynamic loading platform. The four cams are powered synchronously by a single motor.

2.2.5 Data Processing and Constitutive Modeling

The data of all tested tissues was filtered and interpolated the same as what was done by Warren (2008). Briefly, the raw data was ordered using a median filter and then every 15th point was retained. In this way, the noise was reduced while maintaining the character of the curves. The periosteum has negligible bending stiffness, and we can reasonably assume a state of plane stress that does not change throughout the thickness to facilitate application of the membrane theory of continuum mechanics. Cauchy stress, $\mathbf{T}$, and Green-Lagrange strain, $\mathbf{E}$, were calculated in Equations 4 and 5, respectively.

$$\mathbf{T} = \frac{1}{\det\mathbf{F}}\mathbf{F}\cdot\mathbf{P} \tag{4}$$

$$\mathbf{E} = \frac{1}{2}(\mathbf{F}^T\cdot\mathbf{F} - \mathbf{I}) \tag{5}$$

$\mathbf{P}$, the Lagrangian stress, also known as the first Piola-Kirchhoff stress, is shown in Equation 6 with L_1 and L_2 corresponding to the circumferential axis and longitudinal axis traction-free lengths, respectively, and $\boldsymbol{f}$ as an axial force.

$$\mathbf{P} = \begin{bmatrix} \frac{f_1}{L_2} & 0 \\ 0 & \frac{f_2}{L_1} \end{bmatrix} \tag{6}$$

The magnitudes of $\mathbf{T}$ and $\mathbf{V}$, where

$$\mathbf{V}^2 = \mathbf{F}\cdot\mathbf{F}^T, \tag{7}$$

were also calculated for all tissues because of noted anisotropy (when tested relative to a relaxed preconditioned state [Warren, 2008]), with a general equation for calculating magnitude using the general tensor $\mathbf{G}$ being

$$|\mathbf{G}| = \sqrt{tr(\mathbf{G}\cdot\mathbf{G}^T)}\,. \tag{8}$$

Finally, the data was interpolated at 0.5 increments of calculated stress, thereby allowing us to create “averaged” curves for various groups of tissue.

Calculated constitutive parameters for tissues tested from a relaxed state were based on data from Constant-X, Constant-Y, and Equibiaxial protocols. Models for samples tested relative to an *in vivo* configuration relied solely on Equibiaxial data. The 2D components of Equation 4 were calculated to fit to the general constitutive relation for a hyperelastic membrane (Equation 9), via Levenberg-Marquardt nonlinear least squares regression in MATLAB.

$$\mathbf{T}_{ij} = \sum_{k=1}^{2}\sum_{p=1}^{2} \frac{1}{\det\mathbf{F}} \mathbf{F}_{ik} \cdot \mathbf{F}_{kp} \cdot \frac{\partial w}{\partial \mathbf{E}_{pj}} \tag{9}$$

The indices i,k,p, and j $\in$ [1,2]. The Fung-type, 2D pseudo strain energy function w is described in Equation 10, 11, and 12 where c_i denotes material constants.

$$w = c_5[(\exp Q_1 - 1) + (\exp Q_2 - 1)] \tag{10}$$

$$Q_1 = \frac{1}{2} c_1 {E_{11}}^2 + c_2 E_{11} E_{22} \tag{11}$$

$$Q_2 = \frac{1}{2} c_3 {E_{22}}^2 + c_4 E_{11} E_{22} \tag{12}$$

Convergence of this model and each set of data was satisfied when the error changed by less than 1E-07 in a single iteration. Each data set produced a group of 5 coefficients.

2.3 Post Processing of Tissues

Fresh tissues, those from mechanical tests, and cultured tissues were fixed in formalin in one of two constraints: *in vivo* or relaxed. For the *in vivo* constraint, the tissue was stretched similar to its *in vivo* dimensions and the media or saline was removed from the chamber and the tissue was completely submerged with formalin to remain for at least 12 hours before transfer from the chamber to histology. For the relaxed constraint, the tissue was removed from the chamber and placed in a Petri dish and submerged in formalin and then sent to histology for processing.

2.3.1 Histological Study

All tissues were sliced on-edge along both longitudinal and circumferential axes (Figure 2.4), yielding cross-sections of the periosteum. Five sections (25 microns) were taken at five levels through the tissue. Of the five sections, one was stained with Hematoxylin and eosin (H&E) to stain cells and structure, one with VVG to stain elastin, one with von Kossa to stain calcium, one with Proliferating Cell Nuclear Antigen (PCNA) to stain active nuclei, and one was left unstained.

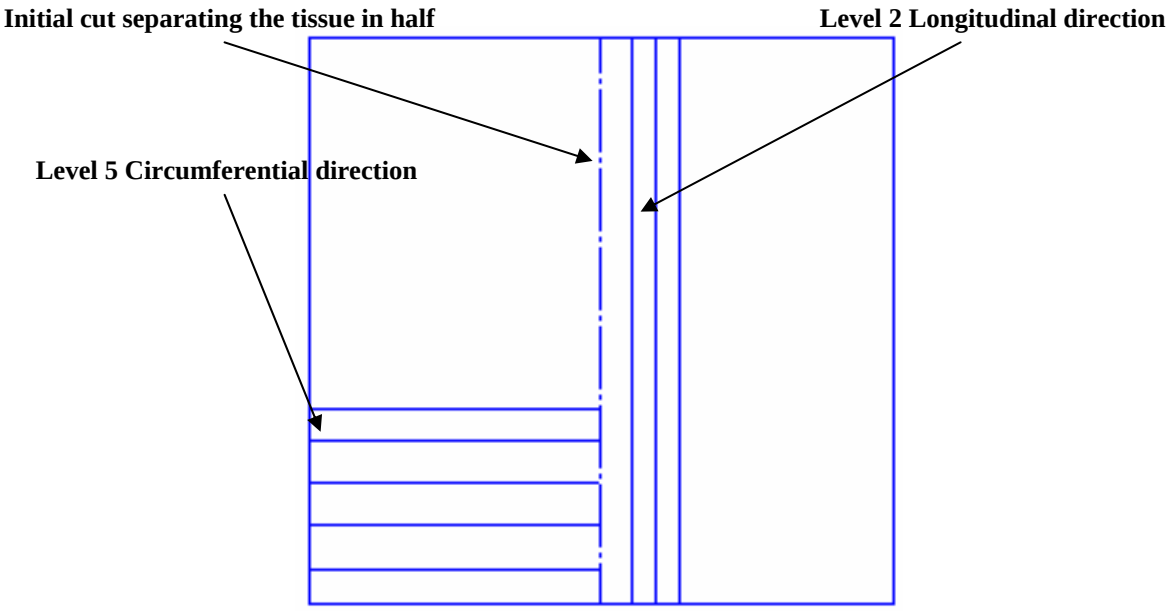

Figure 2.4 Locations of examined for histology slices (figure not drawn to scale). Levels were selected closest to the central region of the tissue

CHAPTER 3

RESULTS

3.1 Native Mechanical Data

The periosteum when tested equibiaxially relative to its preconditioned reference configuration, β_P, was shown to have a highly anisotropic and nonlinear response [Warren 2008]. Our results show the same behavior (Figure 3.1). There is great stiffness in the circumferential direction, and stress in the longitudinal direction appears to be miniscule, even at the highest obtained stretch. However, when tested equibiaxially relative to its *in vivo* reference configuration, β_{iv}, tissues generally appeared more isotropic, with somewhat isolated cases of a highly anisotropic response with more stiffness in the circumferential direction (Figure 3.2 and Figure 3.3). Circumferential and longitudinal stresses at a stretch ratio of 1.0 are statistically similar (Table 3.1).

Recall that there was no control of age, weight, and sex of pigs tested. In order to ensure the 6 pigs used were similar in mechanical response, the magnitudes of the right stretch tensor were averaged for each pig and compared to one another. The averaged magnitudes of tissues obtained from each respective pig were compared against one another using a standard Z-test, and were all grouped to show statistical similarity when alpha = 0.5 (see Table 3.1). Similarity was shown with Z-values within the range of $1.96 \geq Z \geq -1.96$.

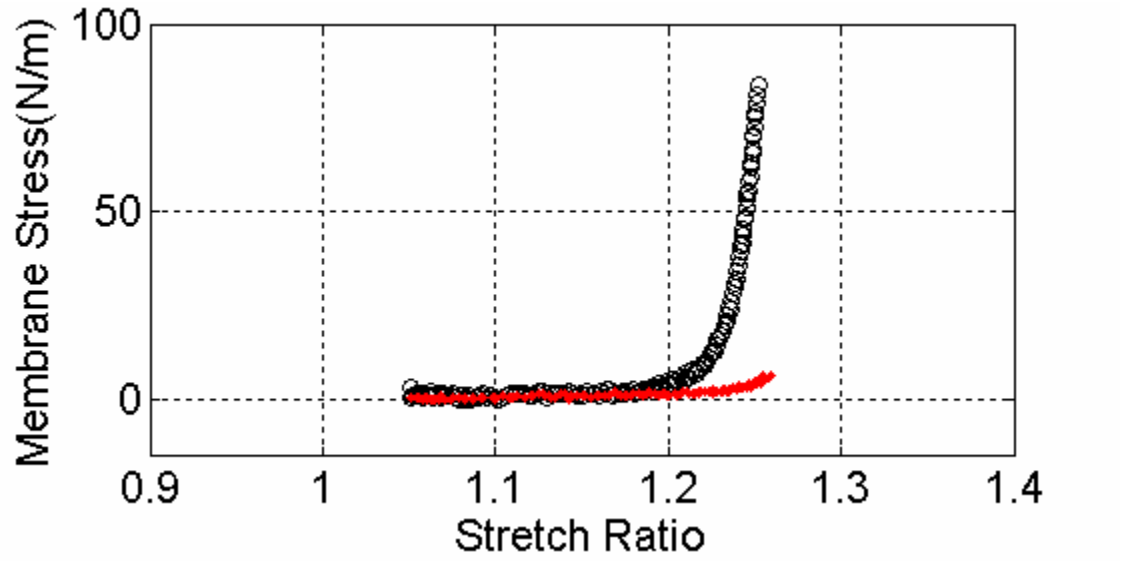

Figure 3.1 Representative mechanical response of tissues tested on Day 0 relative to a preconditioned state β_P. Stiffness is much greater in the circumferential direction. Longitudinal (Red •) and Circumferential (Black O)

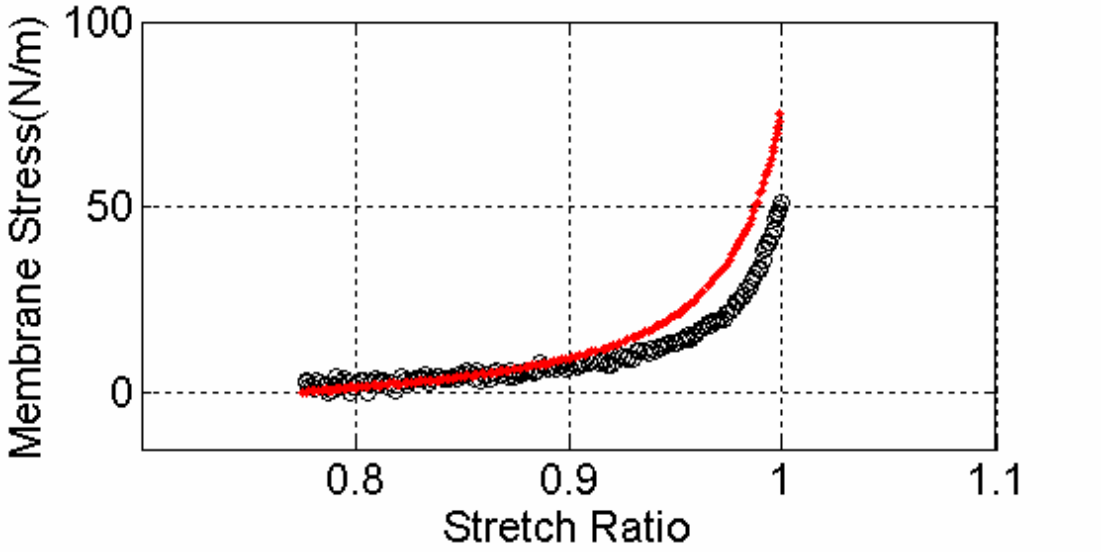

(a)

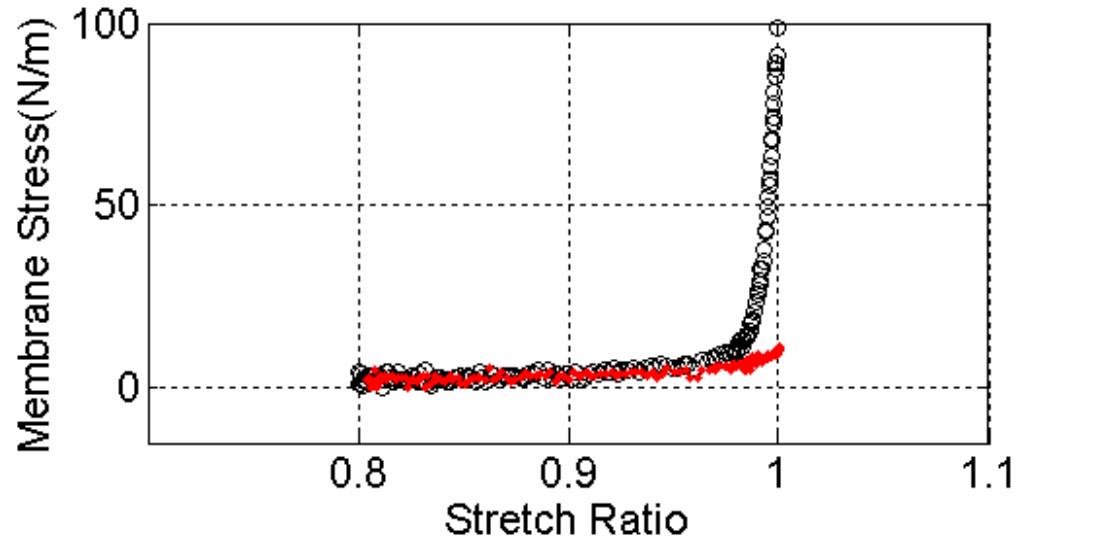

(b)

Figure 3.2 Typical mechanical responses of tissues tested on Day 0. Most tissues showed (a) a relatively isotropic response, and (b) few tissues showed the traditional anisotropic behavior when tested relative to β_{IV}. A stretch ratio of 1 corresponds to tissues approximate *in vivo* dimensions. Longitudinal (Red •) and Circumferential (Black O)

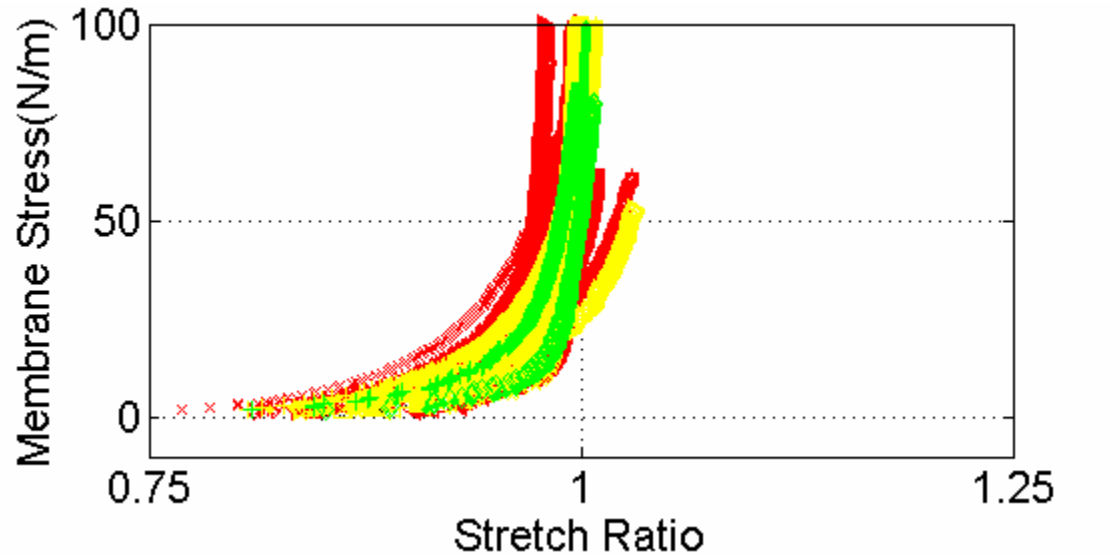

(a)

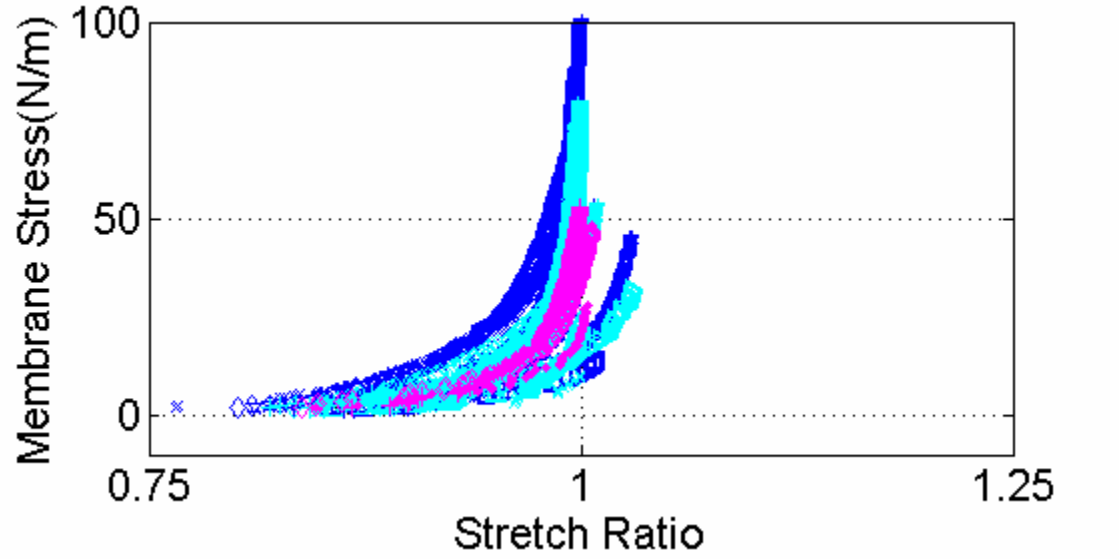

(b)

Figure 3.3 Compiled plots of all day 0 data relative to β_{IV} for (a) circumferential and (b) longitudinal axes. The response in the longitudinal axis has generally higher stresses then stresses relative to a preconditioned state. Some curves go beyond 1.0 because the *in vivo* protocol was limited by an upper load as opposed to a stretch of 1.0.

Table 3.1 Statistical comparison of averaged stretch magnitude means and membrane stresses using 1.96 ≥ Z ≥ -1.96 to represent statistical similarity at alpha=0.5.

	Mean	Standard Deviation	Number of Samples		Statistical Comparision	Z-value	At alpha = 0.5, means are
Circumferential (Membrane Stress N/m)	67.535	42.240	28		Circumferential - Longitudinal	0.270	Similar
Longitudinal (Membrane Stress N/m)	64.871	30.660	28				
					Pig 1-Pig 2	0.079	Similar
					Pig 1-Pig 3	-0.947	Similar
					Pig 1-Pig 4	-0.968	Similar
					Pig 1-Pig 5	0.837	Similar
Pig 1 (|V|)	1.872	0.084	3		Pig 1-Pig 6	0.148	Similar
Pig 2 (|V|)	1.868	0.048	4		Pig 2-Pig 3	-1.138	Similar
Pig 3 (|V|)	1.955	0.145	4		Pig 2-Pig 4	-1.155	Similar
Pig 4 (|V|)	1.958	0.182	6		Pig 2-Pig 5	0.951	Similar
Pig 5 (|V|)	1.811	0.136	6		Pig 2-Pig 6	0.109	Similar
Pig 6 (|V|)	1.862	0.123	5		Pig 3-Pig 4	-0.030	Similar
					Pig 3-Pig 5	1.581	Similar
					Pig 3-Pig 6	1.027	Similar
					Pig 4-Pig 5	1.593	Similar
					Pig 4-Pig 6	1.047	Similar
					Pig 5-Pig 6	-0.652	Similar

3.2 Microstructure

Recall that some tissues were fixed either relaxed or stretched (*in vivo*) on Day 0 and on Day 7 post-testing protocols. Histology slices were obtained from fixed relaxed tissues (Figure 3.4 and Figure 3.6) and stretched (*in vivo*) tissues (Figure 3.5 and Figure 3.7). Care was taken to capture regions close to the center of the tissue where markers were tracked and strain was measured. The longitudinal slices go along the axis of the bone, and the circumferential slices go around the bone. The figures presented are representative for all tissues tested on Day 0 and Day 7. Day 2 histology was not observed. Three layers of the periosteum identified are the cambium (cellular), elastin-rich, and large collagen layer, with the cambium being closest to the surface of bone. Structurally, the relaxed tissues appear to have elastin oriented predominantly in the longitudinal direction (Figure 3.4), and large collagen fibrils oriented in the circumferential direction (Figure 3.6). The undulations of the elastin-rich layer of the longitudinal slice are minute compared the undulations found in the collagenous layer of the circumferential

slice, but are more numerous. Stretched tissues exhibit similar layers to those found in unconstrained tissues. Undulations of the elastin-rich layer in the longitudinal direction are virtually nonexistent; however, yet the collagenous fibers appear to remain slightly crimped along the circumferential axis.

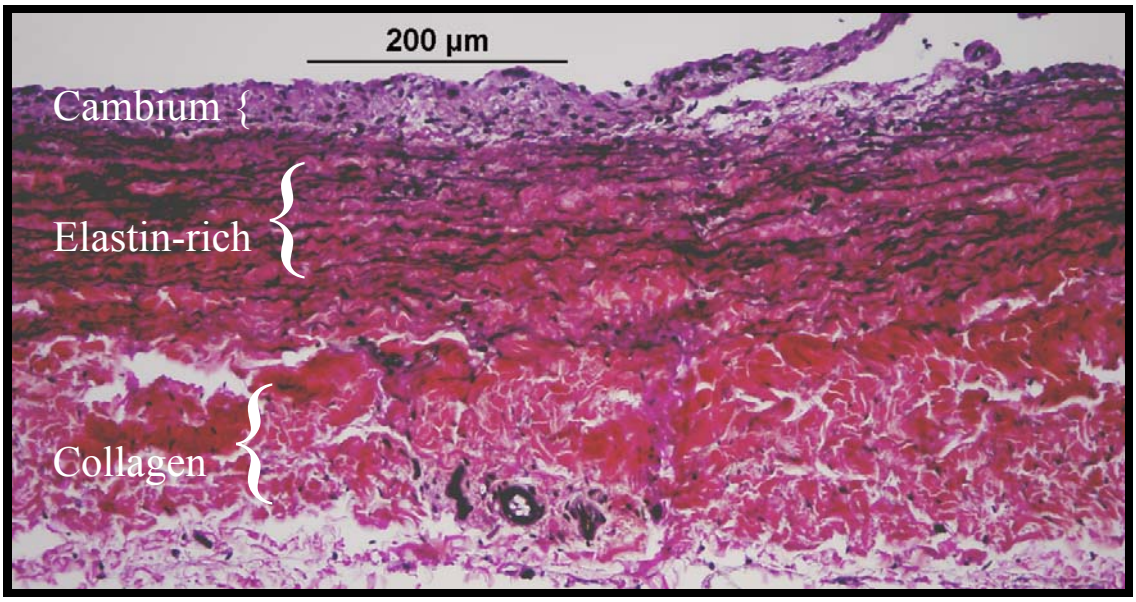

Figure 3.4 Longitudinal slice of an unconstrained, relaxed, periosteal tissue. Elastin fibers appear to be oriented along the longitudinal axis of the bone, collagen fibers appear discontinuous.

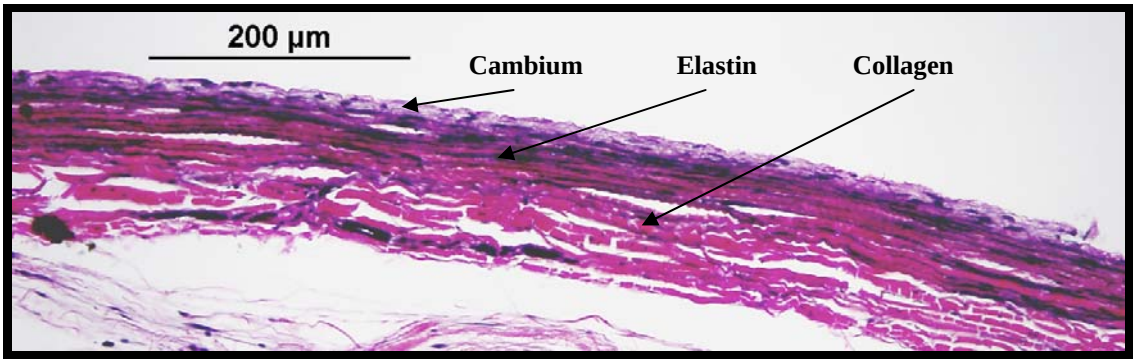

Figure 3.5 Longitudinal slice of a periosteal tissue stretched to its *in vivo* configuration, β_{IV}. Elastin fibers appear to be oriented along the longitudinal axis of the bone, collagen fibers appear discontinuous.

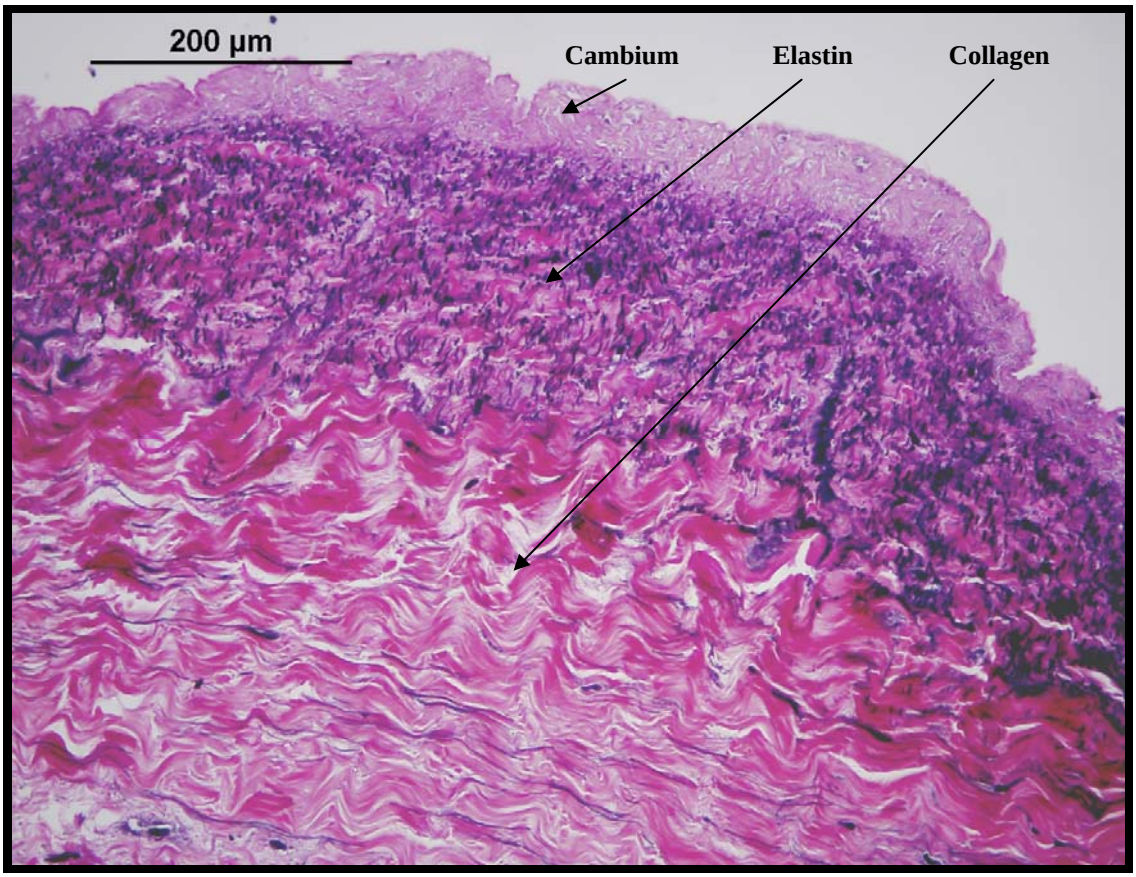

Figure 3.6 Circumferential slice of a relaxed periosteal tissue. Collagen fibers are shown wavy along the circumferential direction of the bone. Elastin appears to be discontinuous and possibly oriented orthogonal to the histological slice.

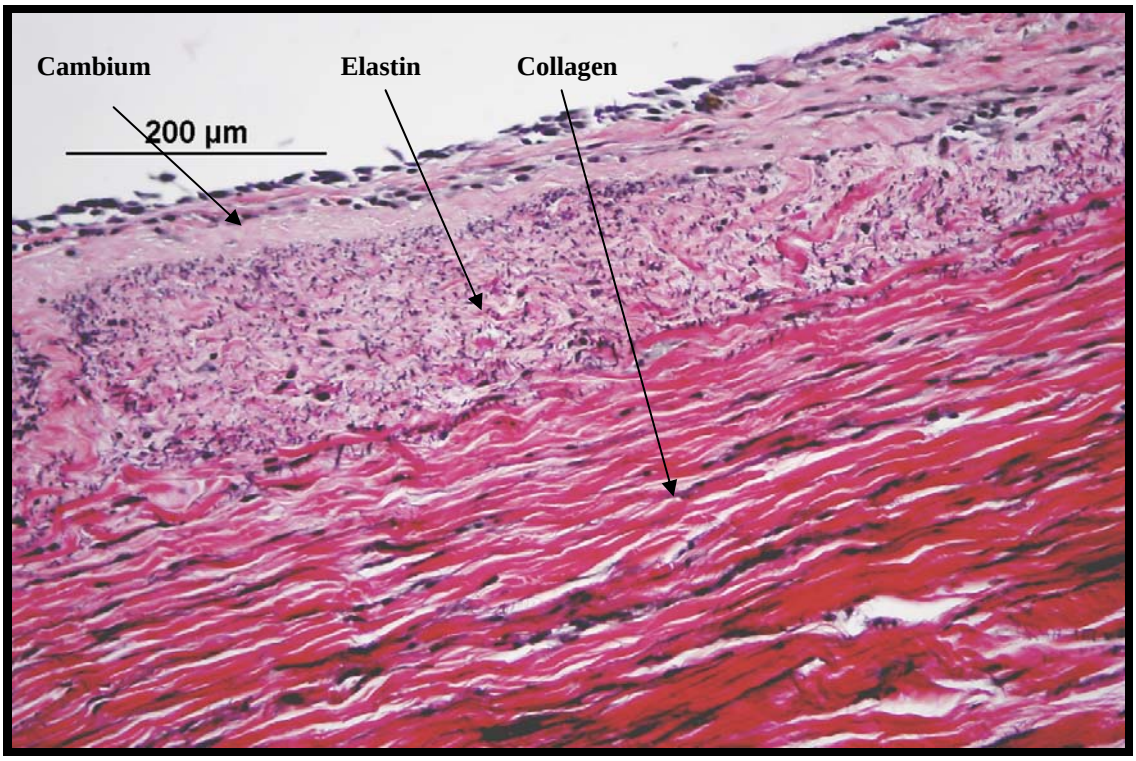

Figure 3.7 Circumferential slice of a periosteal tissue stretched to its *in vivo* configuration, β_{IV}. Collagen fibers are stretched along the circumferential direction, but remain slightly crimped.

3.3 *In Vitro* Remodeling

3.3.1 Reference Configurations

Recall that twelve samples from Day 0 tests were monitored for *in vitro* remodeling, and were also tested on Day 2 and again on Day 7. Mechanical data for one sample on Day 7 was not obtained due to bacterial contamination. Each tissue was tested in reference to their respective day's preconditioned reference. For practical purposes, a reference configuration for each lambda describing a tissue was converted to a single magnitude value and their percent changes between Day 0 and Day 2 and Day 0 and Day 7 reference values were calculated, and the averaged magnitudes of preconditioned configurations of tissues were compared against one another using a standard Z-test. Similarity was shown with Z-values within the range of $1.96 \geq Z \geq -1.96$ (Table 3.2). A negative percentage change is indicative of shrinkage/contraction, and positive percentage change is indicative of growth/extension in

dimensions. Most consistently noted is the trend in the tissues under the relaxed constraint, which appear to shrink over time. The dynamic constraint exhibited the most difference between days, the means shows shrinkage/contraction at Day 2 and also growth/extension at Day 7.

Table 3.2 Percentage Changes of β_P between Day 0 and Day 2 and Day 0 and Day 7 in Magnitude Preconditioned Reference Configurations. Statistical comparisons of means for grouped constraints according to magnitude preconditioned reference configurations using 1.96 ≥ Z ≥ -1.96 to represent statistical similarity at alpha=0.05.

Constraint	Comparison of Days	Percent Difference	Number of Samples		Statistical Comparision	Z-value for comparison of |V|	At alpha = 0.5, means are
Relaxed	Day 0 to Day 0	0%	4				
	Day 0 to Day 2	-5.855%	4		Day 0-Day 2	2.803	Dissimilar
	Day 0 to Day 7	-5.843%	4		Day 0-Day 7	6.435	Dissimilar
	Day 2 to Day 7	0.013%	4		Day 2-Day 7	-0.005	Similar
In Vivo	Day 0 to Day 0	0%	5				
	Day 0 to Day 2	-1.297%	5		Day 0-Day 2	1.989	Dissimilar
	Day 0 to Day 7	-2.183%	4		Day 0-Day 7	1.506	Similar
	Day 2 to Day 7	-0.898%	4		Day 2-Day 7	0.557	Similar
Dynamic	Day 0 to Day 0	0%	3				
	Day 0 to Day 2	-4.281%	3		Day 0-Day 2	2.143	Dissimilar
	Day 0 to Day 7	4.345%	3		Day 0-Day 7	-2.475	Dissimilar
	Day 2 to Day 7	9.011%	3		Day 2-Day 7	-3.244	Dissimilar

3.3.2 Changes in Mechanics

The mechanics of twelve tissues tested relative to a preconditioned state was monitored over time. Averaged magnitude data for Day 0 is shown in Figure 3.8, where |T| is membrane stress magnitude and |V| is the magnitude of the right stretch tensor. The averaged |V| reached was approximately 1.91 which is approximately 1.35 for both lambdas. Figure 3.9 shows grouped data averages (according to day tested) for different constraints. Relaxed and *in vivo* constraint data show gradual increases in magnitudes over time, whereas dynamic constraints show a more extensible response on Day 2 and a less extensible response on Day 7. The averaged magnitude stretch of tissues obtained from each respective day was compared against one another within grouped constraints using a standard Z-test. Similarity was shown with Z-values within the range of 1.96 ≥ Z ≥ -1.96. Statistical similarities are shown between

each respective day's mechanics, except between Day 0 and Day 7 for relaxed constraints (Table 3.3). Tissues were confirmed as viable at Day 7 from PCNA stained slices, indicated by Figure 3.10, where the dark brown indicates proliferating cell nuclei. Qualitative comparisons between PCNA slices showed no difference for all stained slices, and tissues exhibited similar characteristics in location of proliferating cells. More specifically, a similar distribution of proliferating cells was also found in freshly fixed periosteum (immediately fixed in formalin post-excision).

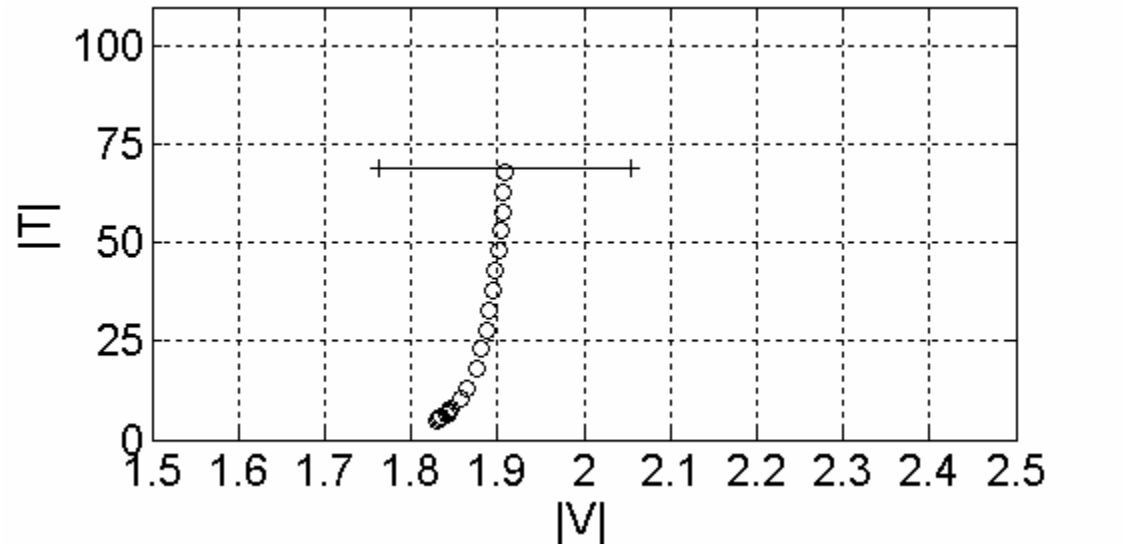

Figure 3.8 Averaged magnitude data for all day 0 tissues. The averaged magnitude |V| reached was approximately 1.91 which is approximately 1.35 for both lambdas.

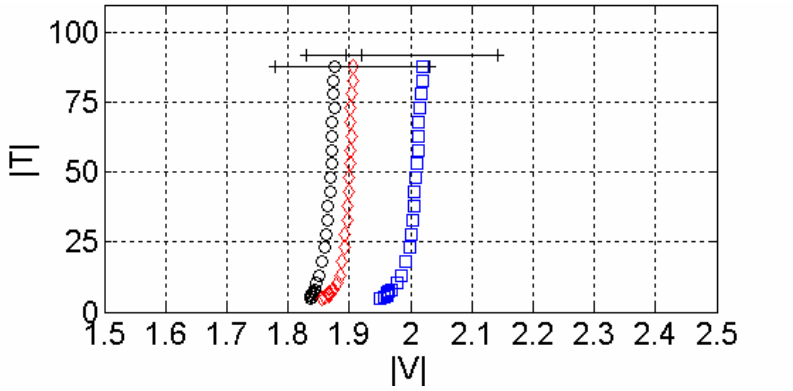

(a)

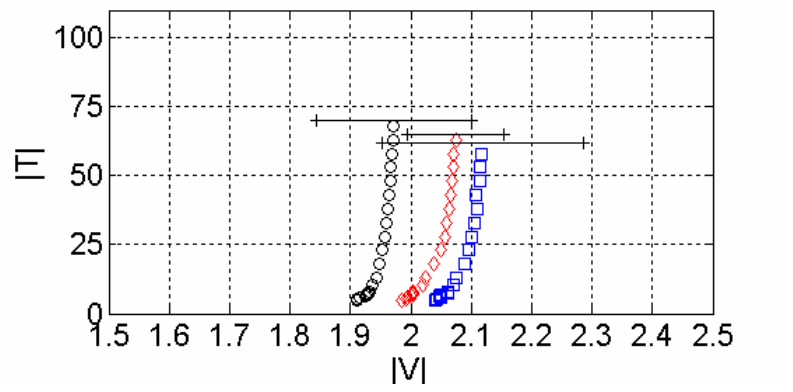

(b)

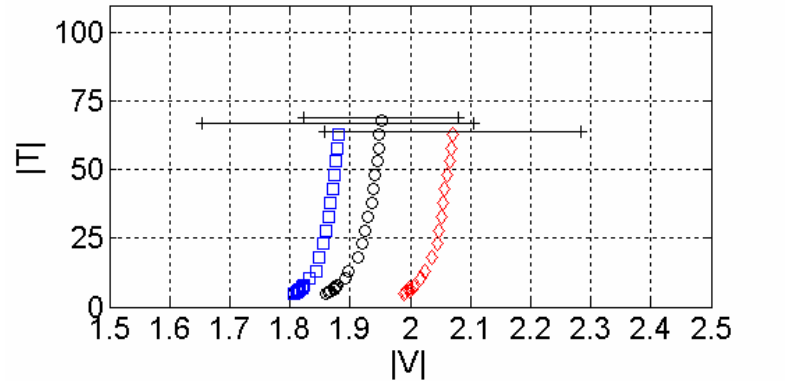

(c)

Figure 3.9 Averaged magnitude data for constraints (a) relaxed, (b) *in vivo*, and (c) dynamic when tested relative to its respective day's recorded preconditioned reference configuration, β_P. Trends toward extensibility are evident in (a) and (b), however (c) shows less extensibility on Day 7. Day 0 (Black O) Day 2 (Red ◊), and Day 7 (Blue □)

Table 3.3 Statistical comparisons of mean magnitudes of stretch for grouped constraints using $1.96 \geq Z \geq -1.96$ to represent statistical similarity at alpha=0.05.

Constraint	Day Tested	Mean	Standard Deviation	Number of Samples		Statistical Comparision	Z-value for comparison of |V|	At alpha = 0.5, means are
Relaxed	Day 0	1.880	0.047	4				
	Day 2	1.912	0.129	4		Day 0-Day 2	-0.464	Similar
	Day 7	2.021	0.125	4		Day 0-Day 7	-2.118	Dissimilar
						Day 2-Day 7	-1.218	Similar
In Vivo	Day 0	1.988	0.119	5				
	Day 2	2.082	0.080	5		Day 0-Day 2	-1.468	Similar
	Day 7	2.128	0.167	4		Day 0-Day 7	-1.417	Similar
						Day 2-Day 7	-0.506	Similar
Dynamic	Day 0	1.954	0.128	3				
	Day 2	2.072	0.213	3		Day 0-Day 2	-0.826	Similar
	Day 7	1.883	0.225	3		Day 0-Day 7	0.471	Similar
						Day 2-Day 7	1.056	Similar

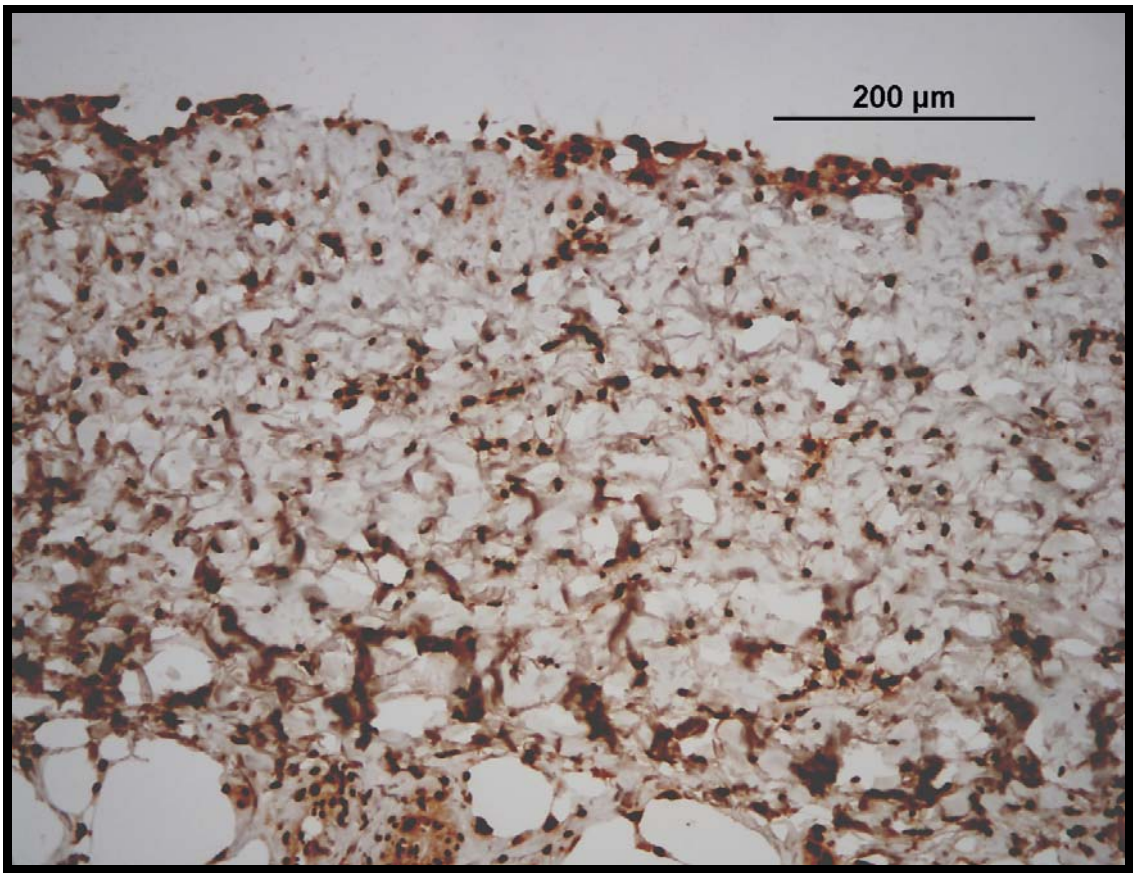

Figure 3.10 Representative slice of a periosteal tissue showing active nuclei. The brown indicates locations of proliferating nuclei.

3.4 Constitutive Modeling

A 5-parameter Fung-type model was found to fit Day 0 data well, and a representative fit is shown in Figure 3.11. However, predictions for the *in vivo* equibiaxial tests (Figure 3.12) and the proportional tests (Figure 3.13) proved unsuccessful, suggesting a better model is needed. Parameter variability is documented for each tissue (Table 3.4), and this could be attributed to any number of tissue-specific characteristics. The constant, c1, typically shows the greatest value and can be attributed to the relative stiffness in the circumferential direction.

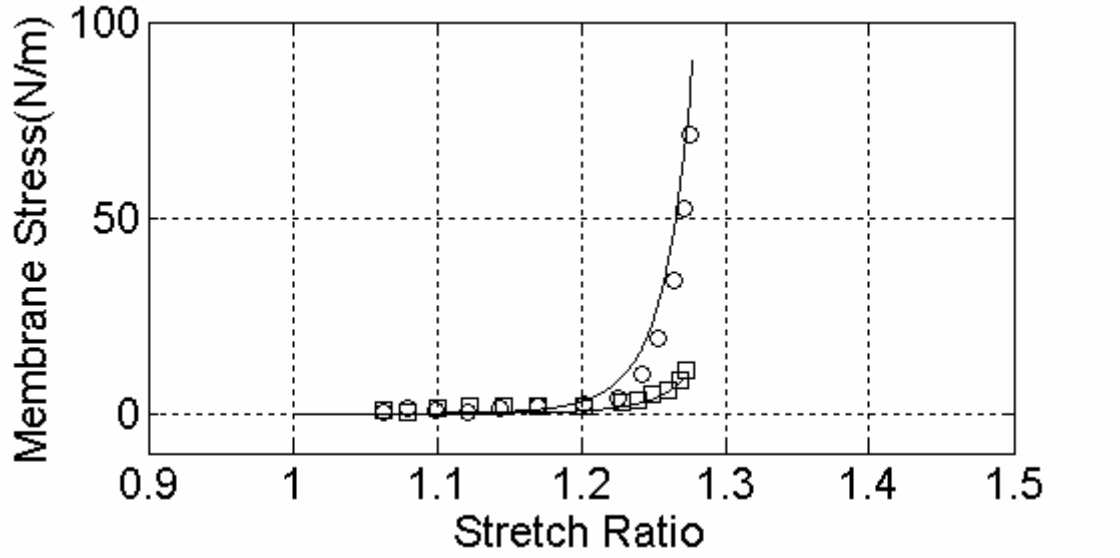

Figure 3.11 Fit of Equation 9 to equibiaxial preconditioned data. The theoretical lines follow along their respective axis of measurement. Longitudinal (Black □) and Circumferential (Black O) Black lines are the theoretical fits.

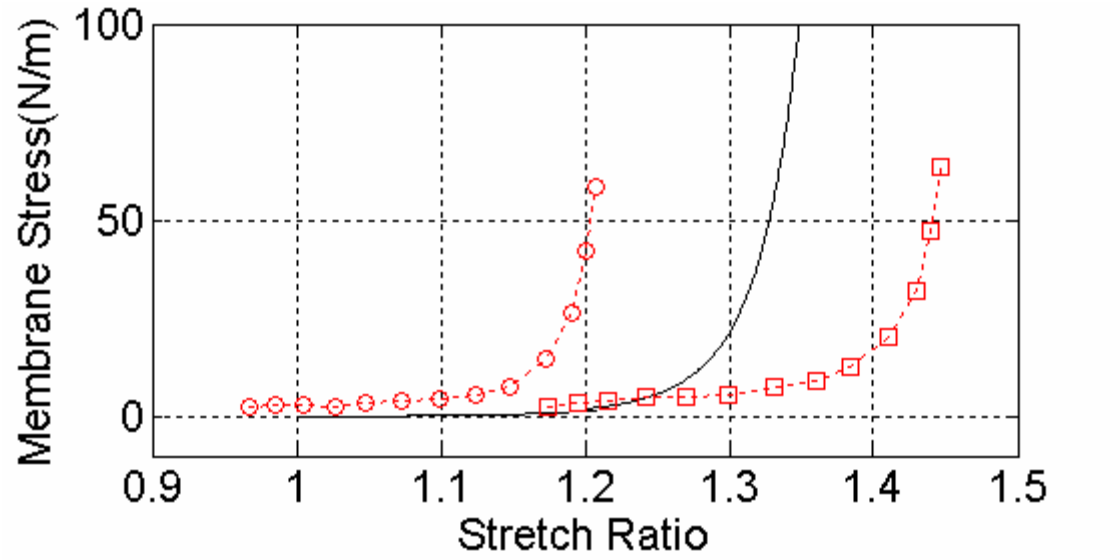

Figure 3.12 Prediction of Equation 9 to *in vivo* data. The theoretical line does not go along either of its respective axes. Longitudinal (Red □) and Circumferential (Red O) Black lines are the theoretical fits.

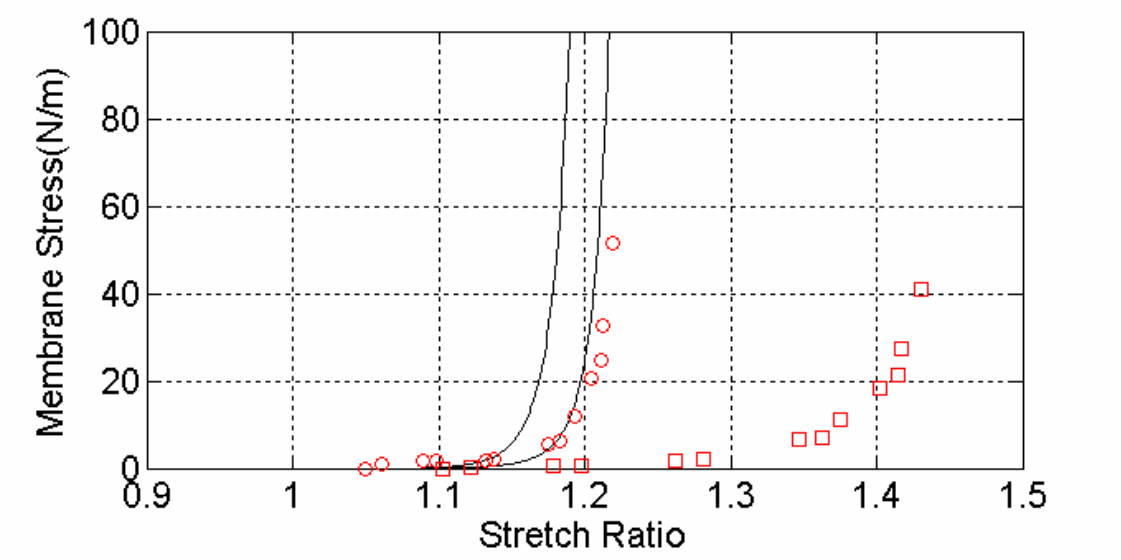

Figure 3.13 Prediction of Equation 9 to proportional data. The theoretical line fits the circumferential axis okay, but fails to do the same for the longitudinal axis. Longitudinal (Red □) and Circumferential (Red O) Black lines are the theoretical fits.

Table 3.4 Coefficient Information for each tissue tested on Day 0. Land R denote left and right limbs, the letters P, M, D, refer to Proximal, Medial, and Distal locations, respectively.

Number	Name	c5 (N/m)	c1	c2	c3	c4
1	RD	0.00034	204.99915	37.68041	0.00000	0.00077
2	LP	0.12734	50.95430	4.29301	0.00000	0.00000
3	LD	0.00073	254.97948	17.28233	0.00000	0.00320
4	RP	0.02033	99.23524	9.05422	53.75440	6.59794
5	LD	0.42246	31.52211	6.82417	18.28687	0.00000
6	LM	0.00003	66.14009	19.60933	0.00000	0.00000
7	RM	0.21383	15.76916	23.69182	23.12827	0.00000
8	RP	0.00212	190.21642	2.25920	103.42101	10.62343
9	LM	0.02186	93.58982	7.33632	0.00000	0.00000
10	RP	0.06317	38.01224	6.65041	14.58285	0.00000
11	LP	0.00335	233.89701	23.51021	0.00000	0.00000
12	RP	0.07830	45.00363	7.30895	0.00000	0.00000
13	RM	1.02536	26.83469	0.00000	15.15146	6.89523
14	LM	0.10011	23.01869	2.87185	0.00000	0.00000
15	LD	0.74379	42.50773	4.12920	14.21416	0.00001
16	LP	0.68885	18.48769	4.61135	10.13724	0.00000
17	RD	0.57242	70.95249	0.00005	21.47659	5.31823
18	RP	0.09944	108.96424	31.02550	0.00000	0.00000
19	LP	0.02922	81.28329	10.13521	0.00000	0.00000
20	RD	0.22250	86.20841	18.90754	14.85072	0.00000
21	LD	0.04807	63.24944	6.70629	0.00000	0.00000
22	RM	0.07626	58.85828	9.61356	29.53445	0.00000
23	RP	0.00061	288.95031	27.99375	0.00000	0.00046
24	LM	0.11324	36.89248	4.34436	22.92792	2.35562
25	RM	0.00044	484.29765	14.28162	210.00019	35.69978
26	LD	0.23813	46.66924	0.00000	7.95359	12.01350
27	LP	0.01756	100.89744	15.48881	56.60547	0.00000
28	RD	0.03596	151.33995	6.65960	62.41493	2.75772
	Average	**0.17735**	**107.63324**	**11.50961**	**24.23000**	**2.93807**
	Std Deviation	**0.26716**	**105.46392**	**10.01649**	**43.93012**	**7.25837**

CHAPTER 4

DISCUSSION

An acute understanding of periosteal mechanics and mechanobiology will go a long way toward improving our conceptions of normal bone growth, as well as improving clinical procedures such as limb lengthening. Herein, we have reported for the first time the mechanical behavior of porcine periosteum near its *in vivo* dimensions, and we have scratched the surface of understanding how those mechanics evolve in response to prescribed mechanical loads.

4.1 Native Biaxial Mechanics

When tested equibiaxially from a relaxed preconditioned state, periosteum has a highly anisotropic, nonlinear mechanical response [Warren, 2008] similar to what has been shown of other collagenous tissues [Chew et al., 1986, Stella and Sacks, 2007]. However, testing protocols relative to an *in vivo* state would potentially provide a better understanding of normal physiology of healthy growth and remodeling, which was our primary focus herein. In doing so, however, we must consider experimental complications that could skew our results.

The *in vivo* configuration for each tissue was determined by back-calculating the stretch ratios from a relaxed configuration to an *in vivo* configuration using the change in gross dimensions from an *in vivo* state to a relaxed state. Some inconsistencies with the measurements may be present, and it was thought that more accurate measurements of the *in vivo* configuration can be obtained with application of markers and capturing of the reference configuration prior to excision. However, this method can prove to be difficult as sterility of the tissue is of utmost importance for monitoring any remodeling or mechanics of the tissue over time, and placement of markers with an unaided eye is impossible without great difficulty. Another note of concern was found during excision; most tissues felt only mildly adhered to the surface of the bone and were removed easily; yet, this behavior was not consistent. Some

samples seemed to be more adhered to the surface of the bone, thus were more difficult to remove. True *in vivo* loads could be affected; however, adhesion of the periosteum to bone has been accounted for previously [Bertram et al., 1998], and is assumed negligible. That said, relative to an *in vivo* state, the periosteum exhibited a more isotropic mechanical response as loads in both directions of stretch were similar, signifying the apparent symmetry for the two testing protocols (reference to *in vivo* versus reference to preconditioned) are different.

At lower stretches, stresses are almost identical in both axes and show only mild deviation from one another at higher stresses. A more gradual transition of membrane stress is prominent for most tissues compared to the sharp transition of the circumferential axis typical of tissues tested relative to a relaxed state. Large variance was found between the loads in the circumferential and longitudinal direction at a stretch ratio of 1, but averaged to comparable stresses (approximately, 65 N/m and 68 N/m). This significant increase in longitudinal stresses, when compared to stresses of samples tested relative to a relaxed configuration, could help expound on why circumferential periosteal sleeve resections increase longitudinal growth [Wilde and Baker, 1987]. Loads in the longitudinal direction have previously been described as mild due to the elastin in that direction [Bertram et al., 1998; Uchiyama et al., 1998], however the results of this study suggest the periosteum maintains a highly stressed state in both directions.

Briefly, Bertram et al. (1998) tested the periosteum intact at its metaphyseal and epiphyseal connections and measured loads at the extension of the periosteum *in vivo*. While novel, this only showed loads in the longitudinal axis and failed to account for stress relaxation that likely occurred due to removal of the diaphysis. Thus, their measurements appear to underestimate true *in vivo* loads. Loads within the periosteum are experienced in both directions, noted by the results of this study and reaffirmed by recent studies involving growing bones [Chen et al., 2008], wherein a correlation between biaxial residual strains and bone growth in the chick embryo tibiotarsus using an isotropic material model was determined. While our results show some isotropic behavior for *in vivo* loads, the behavior was not fully isotropic.

The composition of the periosteum has been documented well [Squier et al., 1990; Allen et al., 2004]. The sources indicate two distinct layers, the “cambium” layer (cellular, osteoblast rich layer, closest to bone) and the structural, collagen and elastin-rich layer. Most recently, porcine periosteum is described as having two distinct structural layers- an elastin-rich collagenous layer, and a collagenous layer with thick fibrils- in addition to the cambium layer [Warren, 2008]. When stretched to an *in vivo* state, the elastin appears to have a greater influence to structural integrity, as indicated by the transition or elbow region of the curve to a highly stressed state being longer in comparison to the smaller transition region noted in periosteum tested relative to a relaxed preconditioned state (see also Kang et al. 1996 for comparison). This greater influence of elastin is supported by the fact that the elastin fibers, oriented preferentially along the axis of the bone, are stretched significantly more when tests are performed relative to the *in vivo* configuration compared to when they are performed relative to the relaxed configuration. This difference in stretch, in turn, has been attributed to the anisotropic tissue shrinkage post-excision [Bertram et al., 1998 Popowics et al., 2002; Warren, 2008]. Though elastin runs preferentially along the longitudinal axis, a gradual transition of the elbow region is also found in the circumferential direction, which may be attributed to some Poisson-type interdependence of the two primary axes. Indeed, our microstructural analysis of periosteum at the *in vivo* state supports these observations.

At high stretches along the longitudinal axis of the bone, the elastin-rich layer seems to be highly stretched as noted by the lack of undulations in the elastin. Similarly, collagen fibers are taut and undulations less pronounced along the circumferential axis. Because these histological slices are indicative of the structure at its greatest stretch (i.e. $\lambda_1 = \lambda_2 = 1$ relative to β_{IV}), we see that the elastin becomes taut prior to the collagen, because the collagen fibrils remain partially crimped, thus supporting elastin’s dominance in our range of stretches. Stated otherwise, strain in the elastin is slowly reduced from a taut state, to a straight uncrimped state,

to a fully crimped state, whereas strain in the collagen is reduced from a mildly crimped state to a fully uncrimped state- never becoming fully taut.

The independence of the two directions tested relative to a relaxed state, as well as the clear delineation of the two structural layers in histology, suggest possible use of a bi-layer constitutive model recently used by Stella and Sacks (2007) that separates the two structural layers and tests them independently. However, there may be some interplay between axes tested relative to an *in vivo* state because of the similarities in loads achieved between the two axes. Therefore, a constitutive Fung-type model was adopted with structural considerations to represent the native mechanics of the tissue.

4.2 Constitutive Modeling

Similar Fung-type models have been employed for the pericardium [Chew et al. 1986], endocardium, and epicardium [Kang et al., 1996], which are comparable structurally to the periosteum. A 7-parameter model was shown to fit well for periosteum [Warren, 2008]. A 4-parameter model [Choi and Vito, 1990] was investigated and was found to fit tissues well with lower extensibility, but was unable to fit higher extensible tissues (not reported). This study used a 5-parameter Fung-type model with an added exponential term to focus on additional contribution found in elastin along the longitudinal axis. The model was found to fit well for most samples but exhibited poor predictability when tested against the tissue's *in vivo* and proportional protocols.

It was noticed that on samples that exhibited slightly more stiffness than usual in the longitudinal axis (samples tested relative to a relaxed state), there were comparable values for parameters c1 and c3. However, wide variability in the constants was found within all tissues samples, and uniqueness of the parameters was not blatantly apparent as variability of coefficients was noticed with the same tissue after multiple fits. This suggests that more structural considerations may need to be used when characterizing the mechanics of periosteum [Lanir, 1979, 1983]. Such a structural model can possibly accompany other

continuum models that describe reorientation of collagen and elastin fibers [Kuhl and Holzapfel, 2007], which is one possible explanation for the changes in the general mechanical behavior of periosteum as it is monitored over time.

4.3 *In Vitro* Remodeling

Changes in apparent symmetry, when tested from an *in vivo* state, were unnoticed for the remodeling aspect of the study, and the tissues remained anisotropic when tested from a relaxed state, for each respective day. However, there were noticeable trends in the averaged data between Day 0 and Day 7 for testing relative to a relaxed preconditioned state. Changes were most notable within the relaxed constraints for preconditioned data and magnitude stretch. This could be attributed to the fact that collagenous tissues shrink or continue to fold into themselves over time due to cell mediated contraction [Anderson et al., 1990; Asaga et al., 1991]. It is also important to note that regardless of the similarity in the percent changes seen in Day 2 and Day 7 of the relaxed constraint tissues (Table 3.2), there is a significant difference in the magnitudes achieved for those respective days because Day 7 tissues shows increased extensibility (Figure 3.9a). Despite statistical similarities, trends in the behavior of the relaxed and *in vivo* constraint are quite evident as the samples appear to become more extensible over time (Figure 3.9b). Dynamic constraints show dissimilarities at all time points showing greater extensibility at Day 2 and less extensibility at Day 7, but it remains unclear as to why the tissue behaves that way. One possible explanation is that the dynamic protocol is destructive to the tissue, yet this runs counter to the observation that tissues become stiffer from Day 2 to Day 7. Regardless, the variability in the averages leads the author to believe that further testing should be completed. Perhaps other forms of microstructural imaging in addition to histological analysis could illustrate a clearer picture as to why tissue behaves a certain way at different time points. Our sample sizes were small for each group, because of several issues of contamination, mostly fungus, which obstructed attempts for the remodeling aspect of the study. This was most likely a result of tissues needing to be removed from their sterile environment to the biaxial

testing system, and back to incubation. Larger sample sizes from similar pigs could capture a better averaged response, especially for the dynamic constraint. All of which will be a focus in our future work.

CHAPTER 5

SUMMARY

The native mechanics of porcine periosteum show a greater influence of elastin in its *in vivo* state, and is shown to be highly stressed contrary to other findings. Histology samples show a visibly lengthened state of elastin when stretched (*in vivo*). The apparent symmetry is dissimilar to the periosteum tested equibiaxially from its relaxed state, since the tissue appears more isotropic when attached to the bone. Careful analysis of tissues tested relative to its (*in vivo*) state could help explain normal bone growth and development. Characterizing that behavior through microstructural analysis would provide better material parameters and is a focus of our future work.

5.1 Future Directions

Future modeling attempts will include structural considerations from better imaging. An SHG (Second Harmonic Generation) study is currently in preparation in conjunction with another lab to analyze each structural layer and to achieve exact orientations of all structural components of the periosteum. Future controlled experiments of cultured periosteum in different mechanical constraints will add to current data, and attempts to constrain tissues for a longer period of time is another direction. Understanding the true mechanics of periosteum is still in a very early stage, but with an appropriate constitutive model, the behavior of periosteum can be characterized fully.

REFERENCES

Al Hussainy HAJ, Jones S, Ali F, Davies AG. Circumferential periosteal sleeve resection for limb length inequality complicated by growth plate tether. European Journal of Orthopaedic Surgery & Traumatology. 2004. 14(3):195-8

Allen MR, Hock JM, Burr DB. Periosteum: biology, regulation, and response to osteoporosis therapies. Bone. 2004 Nov;35(5):1003-12.

Anderson SN, Ruben Z, Fuller GC. Cell-mediated contraction of collagen lattices in serum-free medium: effect of serum and nonserum factors. In Vitro Cell Dev Biol. 1990 Jan;26(1):61-6.

Asaga H, Kikuchi S, Yoshizato K. Collagen gel contraction by fibroblasts requires cellular fibronectin but not plasma fibronectin. Exp Cell Res. 1991 Mar;193(1):167-74.

Bertram JE, Polevoy Y, Cullinane DM. Mechanics of avian fibrous periosteum: tensile and adhesion properties during growth. Bone. 1998 Jun;22(6):669-75.

Billiar KL, Sacks MS. Biaxial mechanical properties of the native and glutaraldehyde treated aortic valve cusp: Part II--A structural constitutive model. J Biomech Eng. 2000 Aug;122(4):327-35.

Birch JG, Samchukov ML. Use of the Ilizarov method to correct lower limb deformities in children and adolescents. J Am Acad Orthop Surg. 2004 May-Jun;12 (3):144-54.

Carter DR, Beaupré GS. Skeletal Function and Form: Mechanobiology of Skeletal Development, Aging and Regeneration. Cambridge University Press. New York, NY. 2001

Carter DR, Beaupré GS, Giori NJ, Helms JA. Mechanobiology of skeletal regeneration. Clin Orthop Relat Res. 1998 Oct;(355 Suppl):S41-55.

Cattaneo R, Villa A, Catagni MA, Bell D. Lengthening of the humerus using the Ilizarov technique. Description of the method and report of 43 cases. Clin Orthop Relat Res. 1990 Jan;(250):117-24.

Chen JC, Zhao B, Longaker MT, Helms JA, Carter DR. Periosteal biaxial residual strains correlate with bone specific growth rates in chick embryos. Comput Methods Biomech Biomed Engin. 2008 Oct;11(5):453-61.

Chew PH, Yin FC, Zeger SL. Biaxial stress-strain properties of canine pericardium. J Mol Cell Cardiol. 1986 Jun;18(6):567-78.

Choi HS, Vito RP. Two-dimensional stress-strain relationship for canine pericardium. J Biomech Eng. 1990 May;112(2):153-9.

Cowles EA, DeRome ME, Pastizzo G, Brailey LL, Gronowicz GA. Mineralization and the expression of matrix proteins during in vivo bone development. Calcif Tissue Int. 1998 Jan;62(1):74-82.

Decker JD, Marshall JJ, Herring SW. Differential cell replication within the periosteum of the pig mandibular ramus. Acta Anat (Basel). 1996;157(2):144-50.

Görtz B, Hayer S, Redlich K, Zwerina J, Tohidast-Akrad M, Tuerk B, Hartmann C, Kollias G, Steiner G, Smolen JS, Schett G. Arthritis induces lymphocytic bone marrow inflammation and endosteal bone formation. J Bone Miner Res. 2004 Jun;19(6):990-8.

Grant AD, Atar D, Lehman WB. The Ilizarov technique in correction of complex foot deformities. Clin Orthop Relat Res. 1992 Jul;(280):94-103.

Grundnes O, Reikerås O. The importance of the hematoma for fracture healing in rats. Acta Orthop Scand. 1993 Jun;64(3):340-2.

Houghton GR, Dekel S. The periosteal control of long bone growth. An experimental study in the rat. Acta Orthop Scand. 1979 Dec;50(6 Pt 1):635-7.

Houghton GR, Rooker GD. The role of the periosteum in the growth of long bones. An experimental study in the rabbit. J Bone Joint Surg Br. 1979 May;61-B (2):218-20.

Humphrey JD. Cardiovascular Solid Mechanics: Cells, Tissues, and Organs. Springer-Verlag Press. New York, NY. 2002

Humphrey JD, Wells PB, Baek S, Hu JJ, McLeroy K, Yeh AT. A theoretically-motivated biaxial tissue culture system with intravital microscopy. Biomech Model Mechanobiol. 2008 Aug;7(4):323-34.

Humphrey JD, Yin FC. A new constitutive formulation for characterizing the mechanical behavior of soft tissues. Biophys J. 1987 Oct;52(4):563-70.

Hunziker EB, Schenk RK, Cruz-Orive LM. Quantitation of chondrocyte performance in growth-plate cartilage during longitudinal bone growth. J Bone Joint Surg Am. 1987 Feb;69(2):162-73.

Hunziker EB, Schenk RK. Physiological mechanisms adopted by chondrocytes in regulating longitudinal bone growth in rats. J Physiol. 1989 Jul;414:55-71.

Ilizarov GA. Clinical application of the tension-stress effect for limb lengthening. Clin Orthop Relat Res. 1990 Jan;(250):8-26.

Johansson N, Saarialho-Kere U, Airola K, Herva R, Nissinen L, Westermarck J, Vuorio E, Heino J, Kähäri VM. Collagenase-3 (MMP-13) is expressed by hypertrophic chondrocytes, periosteal cells, and osteoblasts during human fetal bone development. Dev Dyn. 1997 Mar;208(3):387-97.

Kang T, Humphrey JD, Yin FC. Comparison of biaxial mechanical properties of excised endocardium and epicardium. Am J Physiol. 1996 Jun;270(6 Pt 2):H2169-76.

Klein-Nulend J, Bacabac RG, Mullender MG. Mechanobiology of bone tissue. Pathol Biol (Paris). 2005 Dec;53(10):576-80.

Kojimoto H, Yasui N, Goto T, Matsuda S, Shimomura Y. Bone lengthening in rabbits by callus distraction. The role of periosteum and endosteum. J Bone Joint Surg Br. 1988 Aug;70(4):543-9.

Kuhl E, Holzapfel GA. A continuum model for remodeling in living structures. Journal of Materials Science. 2007 42(21):8811-23.

Lanir Y, Lichtenstein O, Imanuel O. Optimal design of biaxial tests for structural material characterization of flat tissues. J Biomech Eng. 1996 Feb;118(1):41-7.

Lanir Y. A structural theory for the homogeneous biaxial stress-strain relationships in flat collagenous tissues. J Biomech. 1979;12(6):423-36.

Lanir Y. Constitutive equations for fibrous connective tissues. J Biomech. 1983;16(1):1-12.

Lynch MC, Taylor JF. Periosteal division and longitudinal growth in the tibia of the rat. J Bone Joint Surg Br. 1987 Nov;69(5):812-6.

Markel MD, Wikenheiser MA, Chao EY. A study of fracture callus material properties: relationship to the torsional strength of bone. J Orthop Res. 1990 Nov;8 (6):843-50.

Moffatt P, Thomas G, Sellin K, Bessette MC, Lafrenière F, Akhouayri O, St-Arnaud R, Lanctôt C. Osteocrin is a specific ligand of the natriuretic Peptide clearance receptor that modulates bone growth. J Biol Chem. 2007 Dec 14;282(50):36454-62.

Pacicca DM, Patel N, Lee C, Salisbury K, Lehmann W, Carvalho R, Gerstenfeld LC, Einhorn TA. Expression of angiogenic factors during distraction osteogenesis. Bone. 2003 Dec;33(6):889-98.

Paley D, Catagni MA, Argnani F, Villa A, Benedetti GB, Cattaneo R. Ilizarov treatment of tibial nonunions with bone loss. Clin Orthop Relat Res. 1989 Apr; (241):146-65.

Paley D. Problems, obstacles, and complications of limb lengthening by the Ilizarov technique. Clin Orthop Relat Res. 1990 Jan;(250):81-104.

Popowics TE, Zhu Z, Herring SW. Mechanical properties of the periosteum in the pig, Sus scrofa. Arch Oral Biol. 2002 Oct;47(10):733-41.

Redlich A, Perka C, Schultz O, Spitzer R, Häupl T, Burmester GR, Sittinger M. Bone engineering on the basis of periosteal cells cultured in polymer fleeces. J Mater Sci Mater Med. 1999 Dec;10(12):767-72.

Robling AG, Castillo AB, Turner CH. Biomechanical and molecular regulation of bone remodeling. Annu Rev Biomed Eng. 2006;8:455-98.

Schoenau E, Neu CM, Rauch F, Manz F. The development of bone strength at the proximal radius during childhood and adolescence. J Clin Endocrinol Metab. 2001 Feb;86(2):613-8.

Squier CA, Ghoneim S, Kremenak CR. Ultrastructure of the periosteum from membrane bone. J Anat. 1990 Aug;171:233-9.

Stella JA, Sacks MS. On the biaxial mechanical properties of the layers of the aortic valve leaflet. J Biomech Eng. 2007 Oct;129(5):757-66.

Takushima A, Kitano Y, Harii K. Osteogenic potential of cultured periosteal cells in a distracted bone gap in rabbits. J Surg Res. 1998 Jul 15;78(1):68-77.

Tenenbaum HC, Palangio KG, Holmyard DP, Pritzker KP. An ultrastructural study of osteogenesis in chick periosteum *in vitro*. Bone. 1986;7(4):295-302.

Tong P, Fung YC. The stress-strain relationship for the skin. J Biomech. 1976;9(10):649-57.

Uchiyama E, Yamakoshi K, Sasaki T. Measurement of mechanical characteristics of tibial periosteum and evaluation of local differences. J Biomech Eng. 1998 Feb;120(1):85-91.

Utvåg SE, Grundnes O, Reikerås O. Effects of lesion between bone, periosteum and muscle on fracture healing in rats. Acta Orthop Scand. 1998 Apr;69(2):177 80.

van der Meulen MC, Huiskes R. Why mechanobiology? A survey article. J Biomech. 2002 Apr;35(4):401-14.

Velazquez RJ, Bell DF, Armstrong PF, Babyn P, Tibshirani R. Complications of use of the Ilizarov technique in the correction of limb deformities in children. J Bone Joint Surg Am. 1993 Aug;75(8):1148-56.

Warrell E, Taylor JF. The role of periosteal tension in the growth of long bones. J Anat. 1979 Jan;128(Pt 1):179-84.

Warren PD. Biaxial Mechanical Characterization of Porcine Periosteum. MS Thesis, University of Texas at Arlington, 2008.

Wilde GP, Baker GC. Circumferential periosteal release in the treatment of children with leg-length inequality. J Bone Joint Surg Br. 1987 Nov;69(5):817-21.

Yasui N, Kojimoto H, Sasaki K, Kitada A, Shimizu H, Shimomura Y. Factors affecting callus distraction in limb lengthening. Clin Orthop Relat Res. 1993 Aug; (293):55-60.

Yiannakopoulos CK, Kanellopoulos AD, Trovas GP, Dontas IA, Lyritis GP. The biomechanical capacity of the periosteum in intact long bones. Arch Orthop Trauma Surg. 2008 Jan;128(1):117-20.

BIOGRAPHICAL INFORMATION

Olumide O. Aruwajoye was born in Jackson, Mississippi and moved to Dallas, Texas at the tender age of four. He pursued higher education at Tulane University in New Orleans, Louisiana where he obtained his Bachelor of Science in Biomedical Engineering. He later decided to pursue a Master of Science in Biomedical Engineering at the University of Texas at Arlington, finishing in August 2009. Much of his work professionally and academically has dealt with orthopedic research. His research interests are in bone and soft tissue mechanics in addition to device design and development. He plans to continue working along those interests as he continues his career.